A novel approach to determine residual stress field during FSW of AZ91 Mg alloy using combined smoothed particle hydrodynamics/neuro-fuzzy computations and ultrasonic testing

Eivani, A. R.; Vafaeenezhad, H.; Jafarian, H. R.; Zhou, J.

DOI
10.1016/j.jma.2020.11.018

Publication date
2021

Document Version
Final published version

Published in
Journal of Magnesium and Alloys

Available online at www.sciencedirect.com

ScienceDirect

Journal of Magnesium and Alloys 9 (2021) 1304–1328

www.elsevier.com/locate/jma

Full Length Article

A novel approach to determine residual stress field during FSW of AZ91 Mg alloy using combined smoothed particle hydrodynamics/neuro-fuzzy computations and ultrasonic testing

A.R. Eivani[a,*], H. Vafaeenezhad[a], H.R. Jafarian[a], J. Zhou[b]

[a] School of Metallurgy and Materials Engineering, Iran University of Science and Technology, Narmak, Tehran, Iran
[b] Department of Biomechanical Engineering, Delft University of Technology, Mekelweg 2, 2628 CD Delft, the Netherlands

Received 28 December 2019; received in revised form 6 August 2020; accepted 16 November 2020
Available online 8 January 2021

Abstract

The faults in welding design and process every so often yield defective parts during friction stir welding (FSW). The development of numerical approaches including the finite element method (FEM) provides a way to draw a process paradigm before any physical implementation. It is not practical to simulate all possible designs to identify the optimal FSW practice due to the inefficiency associated with concurrent modeling of material flow and heat dissipation throughout the FSW. This study intends to develop a computational workflow based on the mesh-free FEM framework named smoothed particle hydrodynamics (SPH) which was integrated with adaptive neuro-fuzzy inference system (ANFIS) to evaluate the residual stress in the FSW process. An integrated SPH and ANFIS methodology was established and the well-trained ANIS was then used to predict how the FSW process depends on its parameters. To verify the SPH calculation, an itemized FSW case was performed on AZ91 Mg alloy and the induced residual stress was measured by ultrasonic testing. The suggested methodology can efficiently predict the residual stress distribution throughout friction stir welding of AZ91 alloy.

Keywords: Friction stir welding (FSW); Smoothed particle hydrodynamics (SPH); Adaptive neuro-fuzzy inference system (ANFIS); Ultrasonic; Residual stress.

1. Introduction

High strength to weight ratio and stiffness of magnesium alloys have made these alloys to be vastly used in many advanced industrial units including aerospace, communication and automobile. According to Mironov et al. [1], beside the advantages of wrought magnesium alloys, as-cast magnesium alloys are with great deal of use due to economic consideration in mass production of engineering components. Kouadri-Henni and Barrallier [2] reported that among the conventional grades of cast magnesium alloys, AZ91 alloy with the exceptional combination of economical castability and desirable mechanical characteristics has been extensively used. Cerri et al. [3] believes that, the demand for use of magnesium alloy is still limited comparing to aluminum and titanium alloys, mainly because of their moderately poor corrosion resistance and low ductility

Friction stir welding (FSW) has gained great requests in different advanced applications for joining different similar/dissimilar alloys in which conventional fusion welding methods is not possible economically. As reviewed by Mishra and Ma [4], the technique was first introduced in 1991 and has found its unique application in different fields of joining and also processing. Current investigations come to the point that FSW is a welding process which can yield high-quality structural joints in diverse dimensions in the form of sheets, shells or even pipes. Nandan et al. [5] and Ma [6] stated

* Corresponding author.
E-mail addresses: aeivani@iust.ac.ir (A.R. Eivani), hossein.vafa@gmail.com (H. Vafaeenezhad).

https://doi.org/10.1016/j.jma.2020.11.018

that the key characteristic of the process is the capability to join parts with no melting as happens in conventional fusion welding (electric arc welding, electron beam, and laser welding). Hence, it is categorized as a solid state welding method. According to Threadgill et al. [7], as a consequence of such joining mechanism, defects such as hot cracks, melt, gas void and shrinkage would no longer occur and the option of joining dissimilar metals and even non-metal components is available. Keeping in mind the concept of FSW, similar technique such as friction stir processing (FSP) and fiction stir channeling (FSC) have been developed by Bhargava et al. [8] and Balasubramanian et al. [9], respectively for surface modification and thin-walled structure production purposes. Despite the advantages, FSW is suffering both with respect to the scientific and technical restrictions which keeps it away from becoming a fully industrialized processing route. The main drawback is the considerable torque and forging force required for bringing material into thermomechanical temperature zone with sufficient plastic flow.

Despite the benefits for joining alloys, the distribution of residual stresses, including both compressive and tensile stresses are inevitable during and after FSW. Buffa et al. [10] expresses that the presence of destructive tensile stresses are responsible for crack formation which should be relieved while the advantageous compressive residual stresses precluding the crack formation are essential in order for the fatigue life to be enhanced. During the course of FSW process, residual stresses have to be considered both in longitudinal and transverse directions. At the same time, according to Bussu et al. [11] for stress analysis and as reported by Steuwer et al. [12] for lifetime predictions, the residual stresses have to be measured to guarantee the safest design of welded structure under in-service static and dynamic loadings.

Many analytical and experimental research studies have been conducted on residual stress measurement from different viewpoints. Kartal et al. [13] regulate the variable residual stresses at the micro-scale level and employed the contour technique to develop a mathematical approach. Coules et al. [14] assess the residual stress mode and tensors by taking the advantage of reconstruction and measurements made in an incompatible joined regions.

Another well-known technique is the hole drilling which is commonly performed by installation of strain gage in a specific designation. In an experimental study carried out by Xu et al. [15], residual stress in Al-Cu alloys was measured both in upper and lower sides of the welded region sampled along the weld-line. Hatamleh et al. [16] estimated stress level and position of stresses in the vicinity of weld and revealed that there exist a linear connection concerning the residual stress with applied force in the case of thin sheets while inserting welding fixtures. In addition to the XRD, Javadi et al. [17] utilized ultrasonic method for residual stress measurements both for fusion and solid state joining processes like FSW, according to. Lu et al. [18] calculated the residual stress state in the Al-Cu fusion welded parts using ultrasonic method. Gachi et al. [19] claimed that considering the sound velocity within the materials, concentrated extreme compressive residual stresses appeared inside the heat affected zone. In the current study, the extent of both longitudinal and transverse residual stresses are measured for AZ91 Mg alloy using an up-to-date procedure based on ultrasonic method.

Application of individual Lagrangian FEM formulation is not a proper choice while dealing with severely straining processes including the FSW as simulation process may stop due to the extreme element distortion. Cervera et al. [20] stated that using FEM simulation merely with Eulerian formulation is not accurate enough as it is unable to precisely monitor the evolution of individual nodes in calculation domain. As an alternative, Arbitrary Lagrangian Eulerian (ALE) was which concurrently preserve calculation domain in Lagrangian mode together with Eulerian meshing strategy. According to Al-Badour et al. [21], ALE is not free of disadvantages as its extra coupled calculations makes simulation longsome, especially in the intrinsically lengthy processes like FSW which leads to some calculation and round-up errors. For tackling such problems taking into account the principles of fluid dynamics, mesh-free approaches solid mechanics such as smoothed particle hydrodynamics (SPH) have been successfully utilized in numerical simulation of many processes including the FSW. Since no classical mesh generation takes place in preprocessing step, relatively large plastic strains can be tolerated throughout numerical computation with nor excessive mesh distortion neither precision error.

According to Liu et al. [22], SPH was initially introduced as a solution for astrophysical problems. Its application filed was successively extended to several fluid [23] and solid mechanic cases such as die casting by Cleary et al. [24], fracture mechanics by Cleary et al. [25], forward extrusion by Cleary et al. [26] and porous media rheology by Jiang et al. [27]. As SPH is fundamentally rooted in Lagrangian calculations and can saves the history of data, problematic phenomena in the view of numerical simulation like void coalescence, reported by Li and Lu [28], or delamination and crack tip opening considered by Randles and Libersky [29] can be analyzed without any additional calculation obstacles while the ability for memorizing thermomechanical history of all calculation elements is kept in place. With respect to the mentioned points, simulation of complex multi-physics cases such as the FSW which includes coupled transient heat transfer, sever plastic deformation at high temperature and fluid flow considering conservation of mass, momentum, and energy can be easily dealt with. Monaghan [30] believed that the key shortcoming of the SPH technique is the dependency on the number of particles (node) as the calculation units are the nodes instead of elements and hence, larger number of points should be assigned in a SPH technique comparing to mesh-based methods.

In this paper, an attempt was made to employ a Lagrangian particle model for FSW of the AZ91 Mg alloy based on the smoothed particle hydrodynamics (SPH) for construction of an appropriate dataset for training and testing of an ANFIS model. The purpose of this work is to establish an integrated SPH-ANFIS model and to validate it against experimental results so that the effect of FSW operational pa-

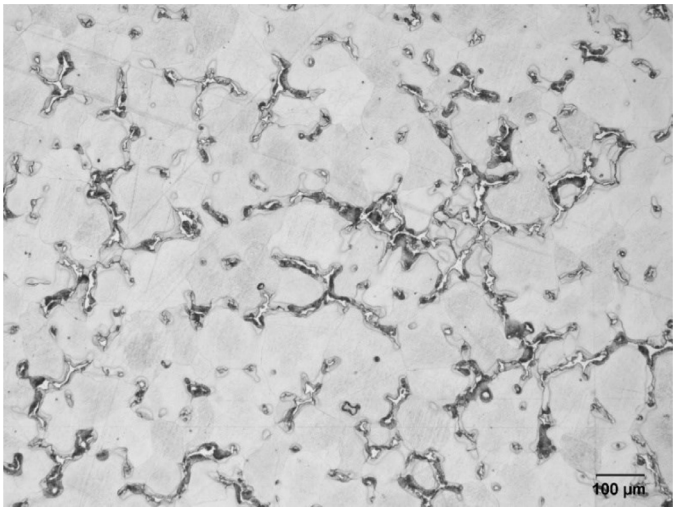

Fig. 1. The micrograph of the as-cast AZ91 Mg alloy.

rameters on the residual stress distribution can be accurately schemed.

2. Materials and methods

The experimental material (AZ91 Mg alloy) was prepared in the as-cast condition. The chemical composition of the material was 8.8Al–1.1Zn–0.13Mn—Mg (wt%). Fig. 1 illustrates the typical as-cast microstructure of the alloy consisting of fine homogenously distributed β particles embedded in magnesium grains. To homogenize the microstructure, β ($Mg_{17}Al_{12}$) precipitates dissolved at 200 °C for 25 h followed by water quenching.

To measure the flow stress of the AZ91 Mg alloy, hot compression test was conducted at different temperatures and strain rates. The test specimens of hot compression, with the diameter of 10 mm and the length of 15 mm were prepared in accordance with ASTM-E209 by wire-cutting from the as-cast material. The hot compression experiments were performed at several temperatures of 300, 350, 375, and 400 °C and strain rates of 0.1, 0.01, and 0.001 s^{-1} at a constant strain of 0.6. Fig. 2 illustrates the true stress–strain curves of the material at the thermomechanical conditions. Prior to isothermal compression testing, the specimens were held at each targeted temperature for 5 min to ensure a homogenous temperature distribution throughout the material. The specimens were then quenched quickly in water immediately after the straining was completed. The quenching was to freeze the microstructure formed at the elevated temperatures. A thin mica layer was inserted to minimize the friction and to prevent the specimen from adhesion to the anvils. A high-precision load-cell with load measuring facility forces was used to record the load-stroke data. The recorded load-stroke data were consequently converted into the true stress–true strain curves using the related standard calculations of mechanical testing.

Plates of the as-cast material, 10 mm thickness, were friction stir welded under different conditions. The rotation speed of 900 rpm and moving speed of 100 mm/min were used to make the FSW joint with a specified initial thermal circumstances i.e. without any preheating. The FSW tool was made of H13 tool steel with a cylindrical pin with 3 mm side length and 5 mm height. Tool shoulder diameter was 15 mm and the tilt angle was 3°. The ultrasonic nondestructive method was used to characterize the induced residual stresses. The frequency of the ultrasonic wave applied was 12.5 MHz while the sound speed in the material is 6000 m/s. keeping in mind the wave length which is equal to 0.5 mm in the transmitter, the penetration depth was estimated as 0.5 mm. The FSW machine and ultrasonic instrumental set-up used in this study are shown in Figs. 3 and 4, respectively.

Table 1
Elastic properties and thermo-physical characteristics of the AZ91 workpiece.

Property	Value	Unit
Young modulus	45	GPa
Poisson ratio	0.33	–
Conductivity	2.09	W/m.k
Heat capacity	84	J/k
Emissivity	0.12	–
Density	1810	kg/m^3

3. SPH numerical simulation of friction stir welding

The commercial finite element software package ABAQUS® 2016 was used in this research to simulate the FSW process of the AZ91 Mg alloy. The developed model consists of deformable $100 \times 100 \times 10$ mm workpiece and a rigid pin, as the workpiece, was considered to have both elastic and plastic behavior and the pin is considered as a discrete rigid part. Since the particle-based SPH formulation was integrated with finite element processor of the software and to avoid the particle run-off and unwanted geometry change in the workpiece, a virtual shell-type die surrounding the workpiece was modeled. The die is to play as a virtual container to preserve the solid boundaries of the sample under thermomechanical loading while the tool rotates and proceeds. The Johnson–Cook plasticity model was used as the appropriate model and the corresponding constants of the model was determined by non-linear least square curve-fitting approach explained in detail in section six. The elastic properties and thermo-physical characteristics of the alloy were extracted from the related literature and listed in Table 1.

Three dynamic steps were defined for simulation of a real-world FSW including the initial plunging phase, the secondary stabilization phase and the final tool movement phase. The non-linear geometry change and the smooth tabular amplitude were implemented in the simulation to avoid extra mesh distortion and instantaneous deformation which leads to convergence. The classical Coulomb's friction model is used to describe the pin/workpiece contact. The friction coefficient μ is set to be 0.3, according to Balasubramanian and Ma [9,4]. All the six rotational and translational degree of freedom of workpiece were set be zero throughout the processing and concurrent rotational and linear velocity were assigned to the

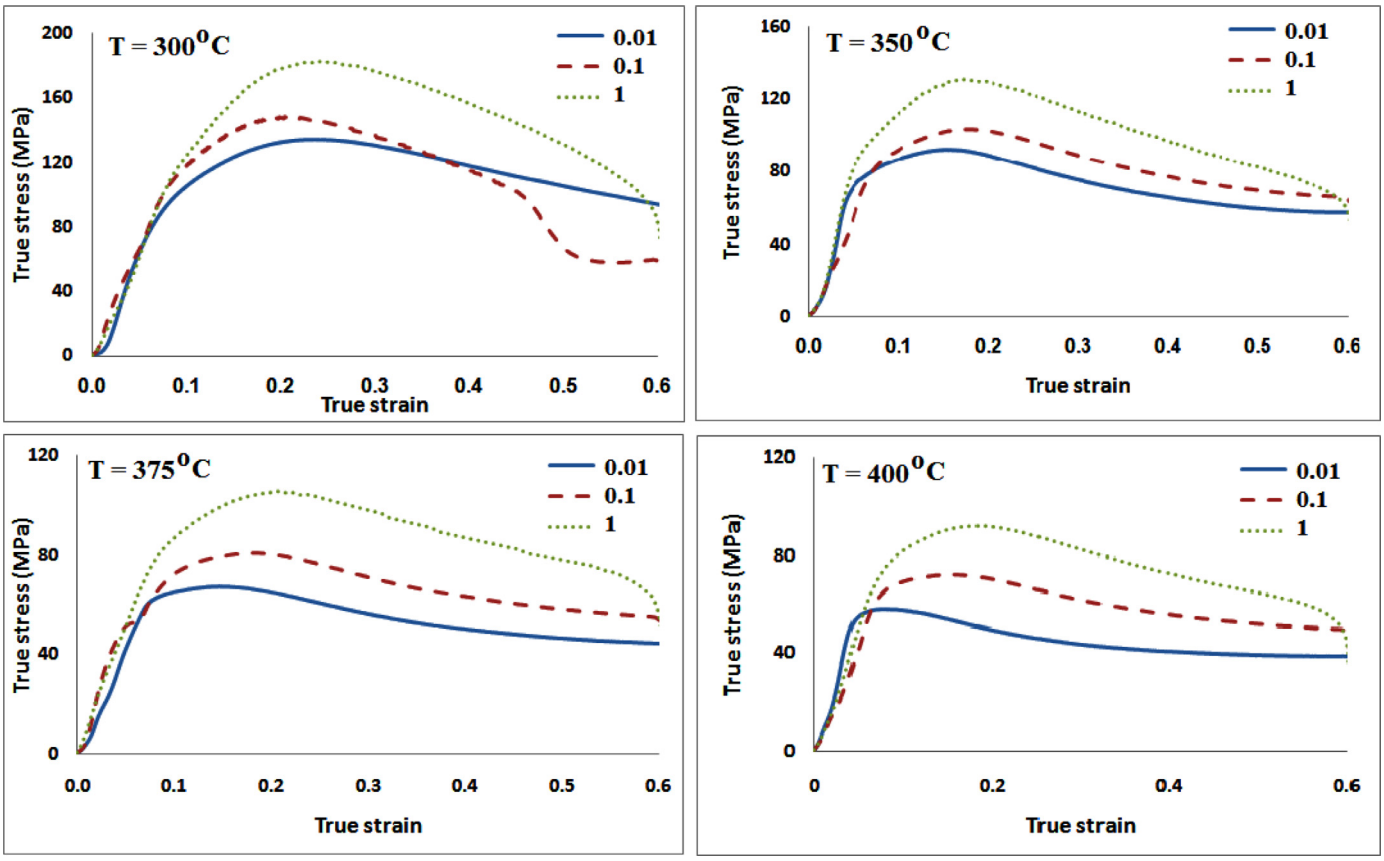

Fig. 2. Hot compression flow stress–strain curves of AZ91 Mg alloy.

Fig. 3. FSW machinery equipment with side clamping facility.

pin. The dynamic explicit method is used to include the dynamic effects in the finite element model. In this method, the factor of mass scaling, which supports the mesh convergence, is considered to be 1000. A larger value can speed up the simulation, but at the same time it may destructively disturb the accuracy of the finite element calculations. The comparison of the kinetic energy against the total internal energy has proven that the mass scaling factor does not affect the accuracy of the model. Fig. 5 shows meshed view of workpiece before starting FSW simulation. Quadratic cubic solid mesh with eight nodes strengthened by reduced integration (C3D8R) and hourglass control utilities were used for mesh generation in pre-processing step. The elements in central region which experience tool contact and its subsequent severe straining are of relatively finer sizes to avoid divergence. In order to collect database for ANFIS model, eighteen FSW simulation were carried out at different welding and preheating conditions. The rotational speeds of 600, 900 and 1200 rpm and moving speeds of 50, 100 and 150 mm/min were assigned to the numerical framework. All the possible combinations of FSW simulation which consider above parameters was performed at both the initial workpiece temperatures of 25 and 100 °C. Some traction points in transverse direction were defined as the tracing units of stress measurement using the "path" facility in FEM software. An overall number of 72 data were gathered to be utilized for ANFIS training and testing steps.

4. Results and discussion

4.1. Determination of Johnson–Cook parameters

The nonlinear least squares problems have been utilized in many real-world challenges including function estimation,

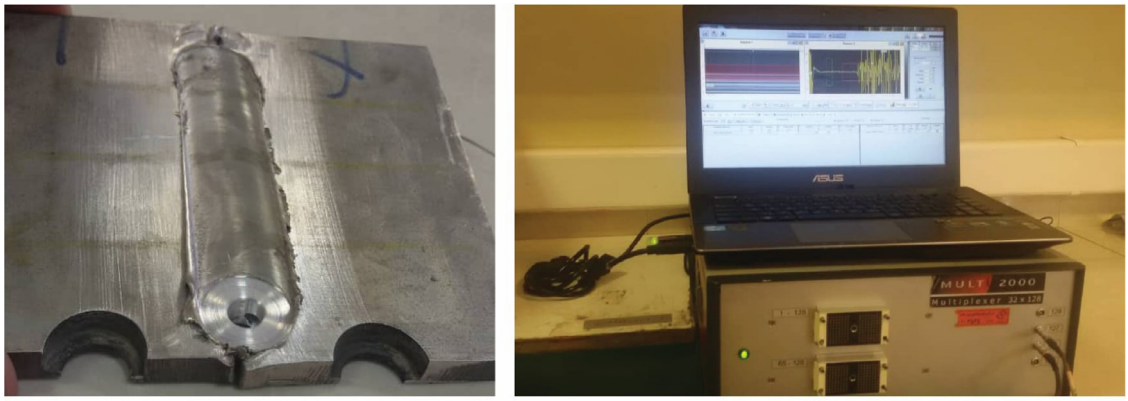

Fig. 4. (a) Sample prepared for stress measurement and (b) Ultrasonic instrumental for residual stress measurement in the as-welded materials.

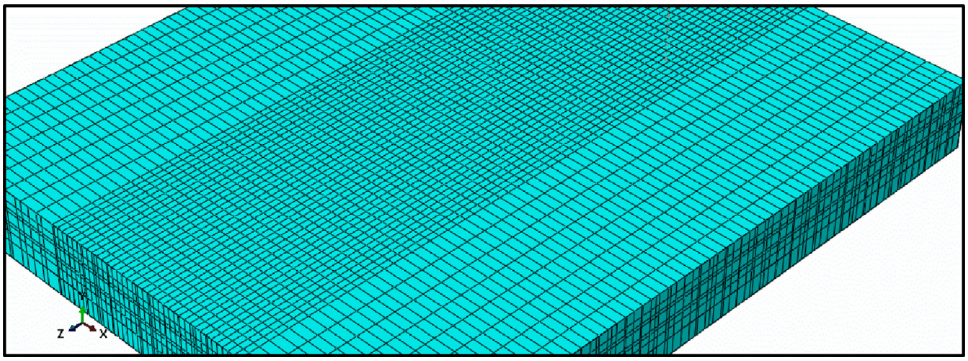

Fig. 5. Solid meshing of the workpiece having two major element sizes at the pre-processing step.

curve-fitting, time series prediction, classification and clustering. The main idea of the non-linear least-squares method is to minimize a real value or numerical function that is summation of a nonlinear functions in terms of its associated variables. In due course, the numerical techniques used rely on the solution of unconstrained nonlinear least squares problems. In a general view, a set of m data points i.e. (x_1,y_1),(x_2,y_2),…, (x_m,y_m) and an initially estimated model function of $y=f(x, \theta)$ have to be assumed. Besides the dependency of variable on the n parameters, $\theta=(\theta_1,\ldots, \theta_n)$ set with the postulation of $m \geq n$ should be also preserved. It is anticipated to identify the corresponding θ parameters in a way that the proposed curve could fit in a superlative mode to the given data in the least squares sense, meaning that the sum of the squares, $\sum_{i=1}^{m} r_i(\theta)^2$ have to approach a minimum value. The Johnson–Cook constitutive model (JC) expresses the flow stress as a function of strain (ε), strain rate ($\dot{\varepsilon}$), and temperature (T). The declared variables express the superimposing effect of thermomechanical parameters i.e. strain hardening, strain-rate hardening and thermal softening, respectively on stress–strain curve. The Johnson–Cook constitutive model is typically defined based on the description mentioned in Eq. (1):

$$Y = \left|A + B\varepsilon_{\mathrm{p}}^{\mathrm{n}}\right|\left|1 + \mathrm{C}\ln\varepsilon_{\mathrm{p}}^{*}\right|\left|1 - \mathrm{T}_{\mathrm{H}}^{\mathrm{m}}\right| \tag{1}$$

$\mathrm{T_H}$ and ε_P^* can be easily calculated by using two bellow terms of Eqs. (2) and (3):

$$\mathrm{T_H} = \frac{(T - \mathrm{T_r})}{(\mathrm{T_m} - \mathrm{T_r})} \tag{2}$$

$$\varepsilon_{\mathrm{p}}^{*} = \frac{\bar{\dot{\varepsilon}}}{\bar{\dot{\varepsilon}}_0} \tag{3}$$

In Eqs. (1) to (3)–(16), A is the room temperature yield stress of the material and ε_p^* is the normalized equivalent plastic strain which is elucidated in terms of $\bar{\dot{\varepsilon}}$ as equivalent plastic strain rate, and $\bar{\dot{\varepsilon}}_0$ as reference strain rate. T_r and T_m are room and melting temperatures of the investigated material, respectively. The term n accounts for the strain hardening influence and m is responsible for the thermal softening, and C is related to the strain rate sensitivity. The applications of the JC model is widespread and is accepted as one of the best deformation model which has been effectively applied for many industrial alloy. In this model, it is assumed that the incremental variation of flow stress is affected merely and concurrently by strain hardening, strain rate effect and thermal softening.

The numerical optimization aimed at finding an arrangement of the JC model constants for the AZ91 magnesium alloy that instantaneously persuade the supplies located on the flow stress as response and related thermomechanical factors.

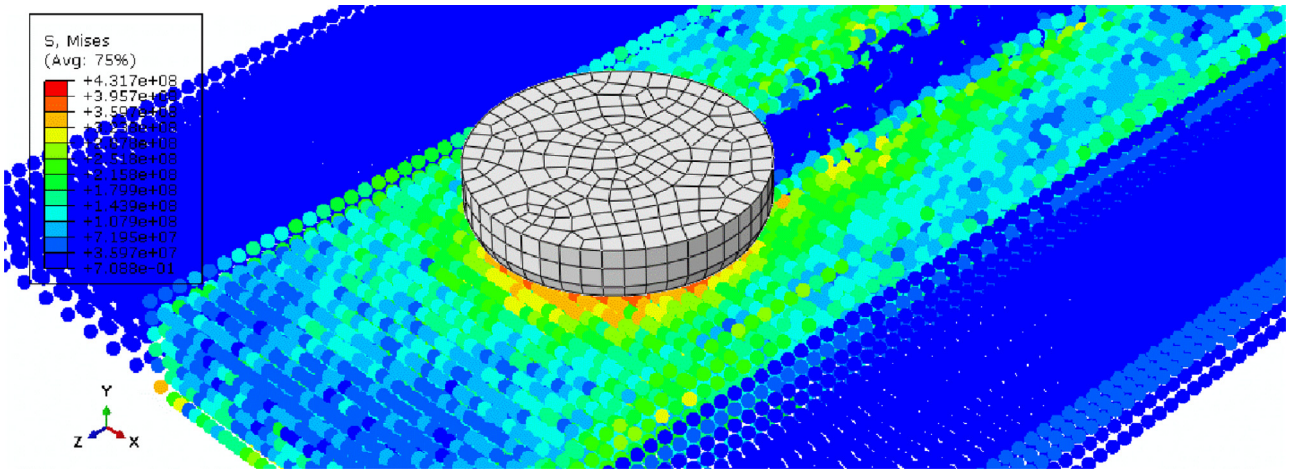

Fig. 6. Particle-based stress calculation of FSW using SPH approach.

Table 2
Johnson–Cook parameters for AZ91 magnesium alloy.

Material	A (MPa)	B (MPa)	C	m	n	T_m (°C)
AZ91 alloy	153	292	0.0766	1.5	0.1026	553

Table 3
Properties used for rigid tool part.

Property	Density	Poisson ratio	Modulus of elasticity
Unit	7850 kg/m^3	0.33	210 GPa

To find out the material-dependent terms in the JC constitutive model should be minimized for the fitting parameter which is defined in the form of Eq. (4):

$$\text{F.P.} = \frac{1}{N}\sum_{i=1}^{N}\frac{|Calculated\ stress - Experimentally\ recorded\ stress|}{Experimentally\ recorded\ stress} \tag{4}$$

The JC parameters for AZ91 magnesium alloy was determined by curve-fitting and consideration of Eq. (4) as the fitness function. The parameters are listed in Table 2. The calculation is preformed to recognize the optimum processing parameters, including the material constants for the JC model, i.e. *A, B, C, m* and n for the minimization purpose. Consequently, the non-linear least square fitting was performed for this optimization resolution. Shortly, the non-linear least square fitting utilizes a fitness function to describe the relationship among the deformation input factors and the flow stress, the output. As, all the input parameters are imported with both a lower and upper limits, a constrained optimization problem is essential and several modifications have to be implemented in the model.

The next step after the determination of Johnson–Cook material model is definition of the equation of state (EOS) to consider the hydrostatic stresses. The stress tensor can be resolved into two independent components of deviatoric and hydrostatic. Applying the EOS, the plasticity can be assumed independent of pressure at low pressure condition and pressure-dependent only at the relatively high pressures. Consequently, the EOS is usually used when the imposed stress state is highly severe to have a comprehensive and precise material model. As severe plastic deformation is applied during the FSW, EOS is necessarily needed to be activated for SPH simulation. To establish an accurate model for in-process analyze of the plastic deformation, the Gruneisen EOS is integrated with the FEM model both in tension and compression stress states. The tool was presumed to stay rigid throughout the FSW joining process. The rigid material model is therefore consorted to the FEM paradigm of the instance to reduce the simulation time period. In case the parameters such as density, modulus of elasticity and Poisson ratio of the rigid instance are not accurately defined, the FEM solving algorithm would encounter with the divergence problem. The properties of the tool used in the present numerical simulation are shown in Table 3.

4.2. Effect of welding/heating parameters on residual stress distribution

The SPH is an applicable Lagrangian method to be utilized for FSW process simulation as it can trace each node in domain to extract the related field outputs. Since, in SPH simulation, the computational units are assumed to be the nodes instead of the elements, heat generation, temperature field, and stress distribution during the process can be easily and truthfully calculated without the risk of element distortion. Moreover, it preserves Lagrangian nature in which nodes can be followed at time-dependent field output. Fig. 6 indicates stress distribution in particle-based SPH simulations in the domain in which nodes which are the calculation unit.

In this research, the effects of two operational factors i.e. rotational speed and moving speed together with preheating temperature were studied on residual stress distributing along the transverse direction of the weld sample. Figs. 7–9 illustrate stress distribution after FSW of the AZ91 alloy at different rotational speeds and constant moving speeds without

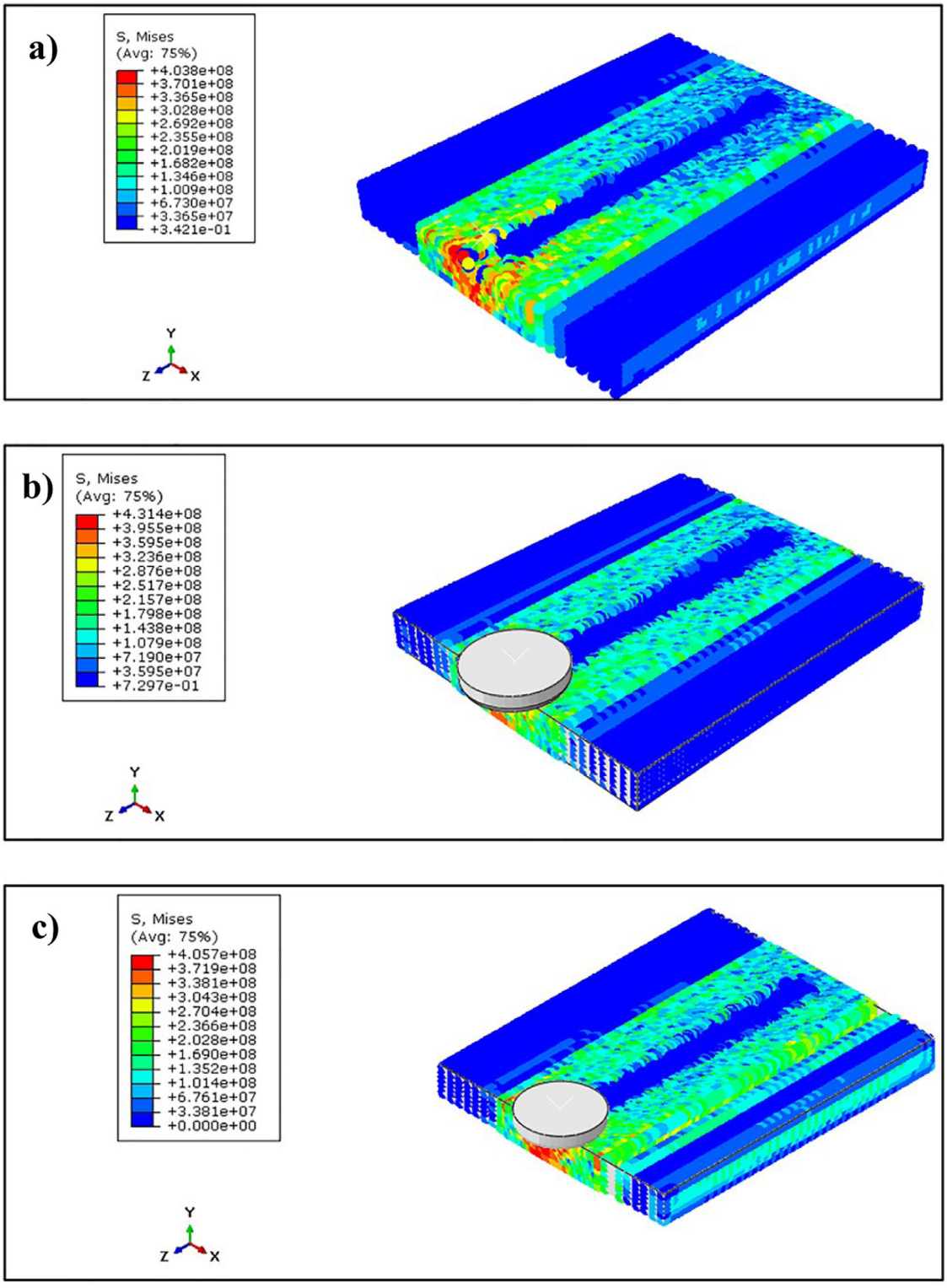

Fig. 7. Residual stress field (Pa) in the welded samples processed at constant moving speed of 100 mm/min and moving speeds of (a) 100 rpm, (b) 50 rpm and (c) 150 rpm. (No preheat).

any preheating. The same situations for the case of 100 °C preheating heat treatment were resulted in Figs. 10–12. The observed trend as a function of tool rotation rate can be rationalized as follows: increasing tool rotation rate enhances the peak temperature in the as-welded material. The extent of thermal load and resulting residual stress would be relatively higher at elevated peak temperature in the material segment of trailing sideways where welding tool effect is highly frailer. This results in a decrease in residual stress. Similarly, a higher peak temperature would widen the weld nugget width increas-

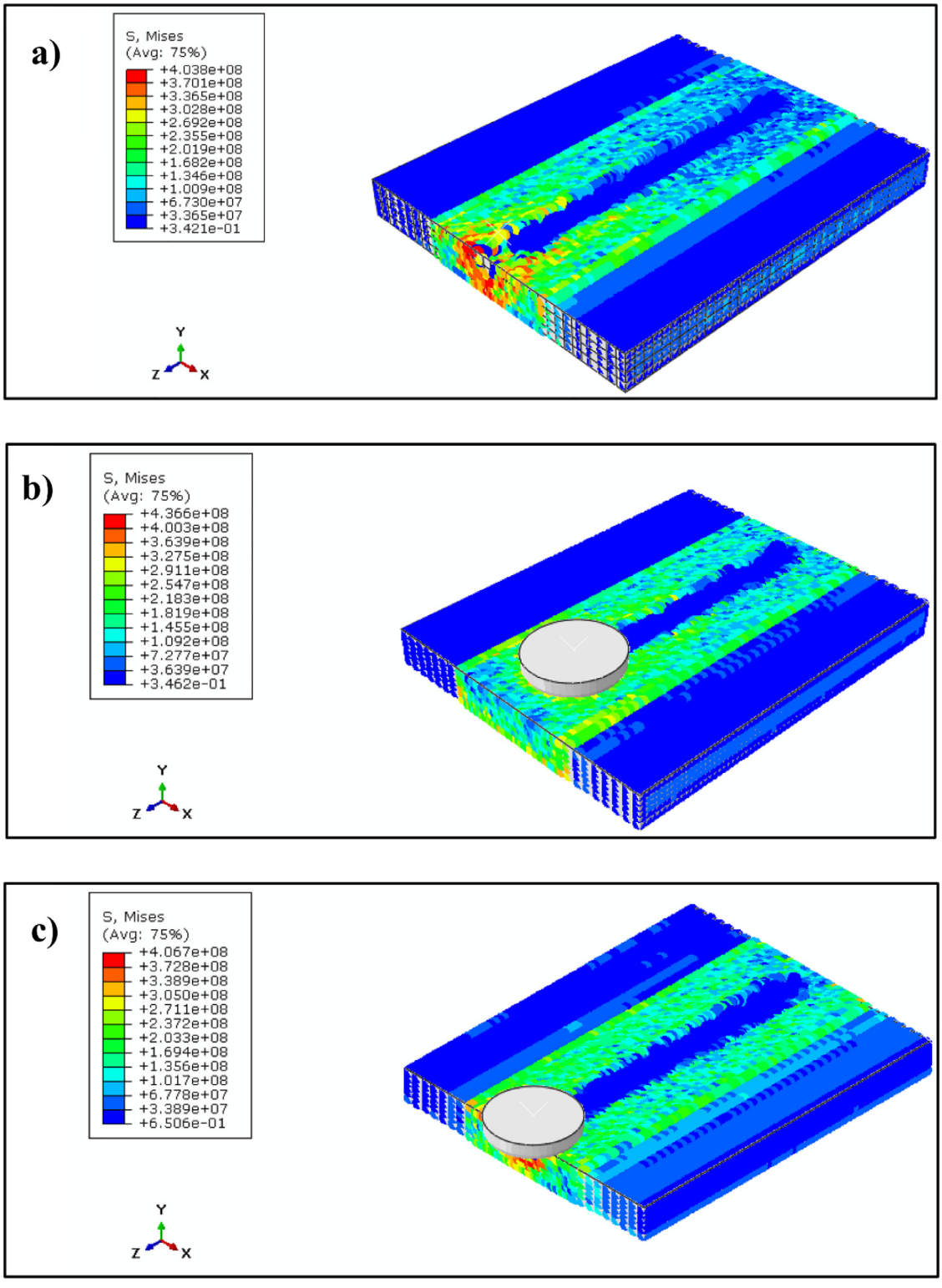

Fig. 8. Residual stress field (Pa) in the welded samples processed at constant moving speed of 50 mm/min and moving speeds of (a) 600 rpm, (b) 900 rpm and (c) 1200 rpm. (No preheat).

ing the width of the zone under longitudinal tensile residual stresses. The heat source formed during tool rotation leads to a concentrated thermal gradient in the base metal zone and thereby an inhomogeneous severe deformation. In the FSW, and at any definite temperature, the zones adjacent to the tool is subjected to thermal stresses approximately equal to the material yield stress. Along the regions behind the passing heat source, the welded material begin losing temperature

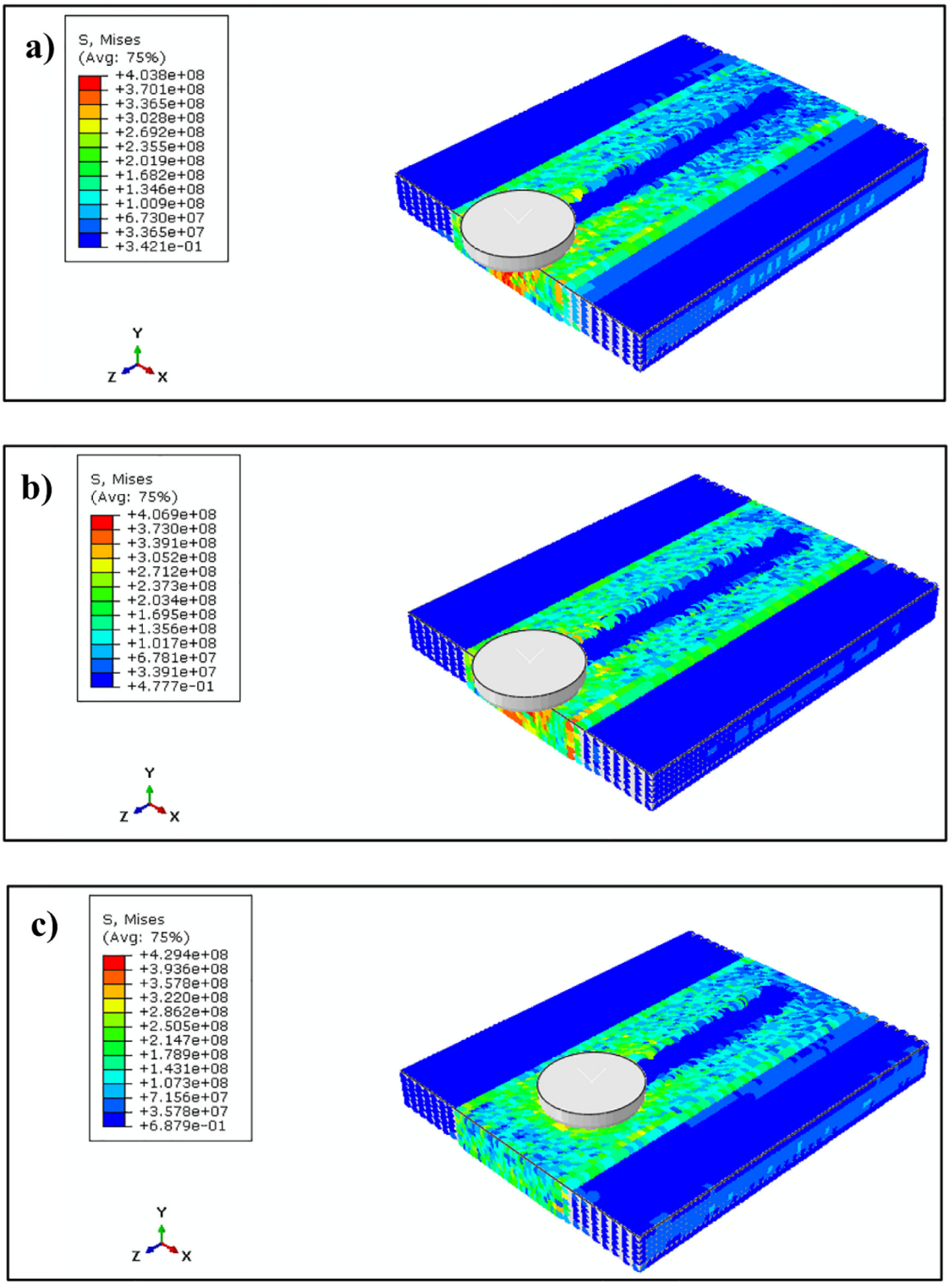

Fig. 9. Residual stress field (Pa) in the welded samples processed at constant moving speed of 150 mm/min and moving speeds of (a) 600 rpm, (b) 900 rpm and (c) 1200 rpm. (No preheat).

and thereby contracting. The vicinal material, however, restricts the contraction of the spot and hence, tensile stresses tends to spawn at place. The farther is the distance from the moving heat source, the higher the magnitude of the generated tensile thermal stress would be. For the zones in front of the heat source, the metal is assumed in its original temperature and thermal stresses are anticipated to be almost zero.

Analogously to the rotation speed, the variation of the tool moving speed gives rise to different residual stresses distributing throughout the welded samples. Figs. 13–15 show changes

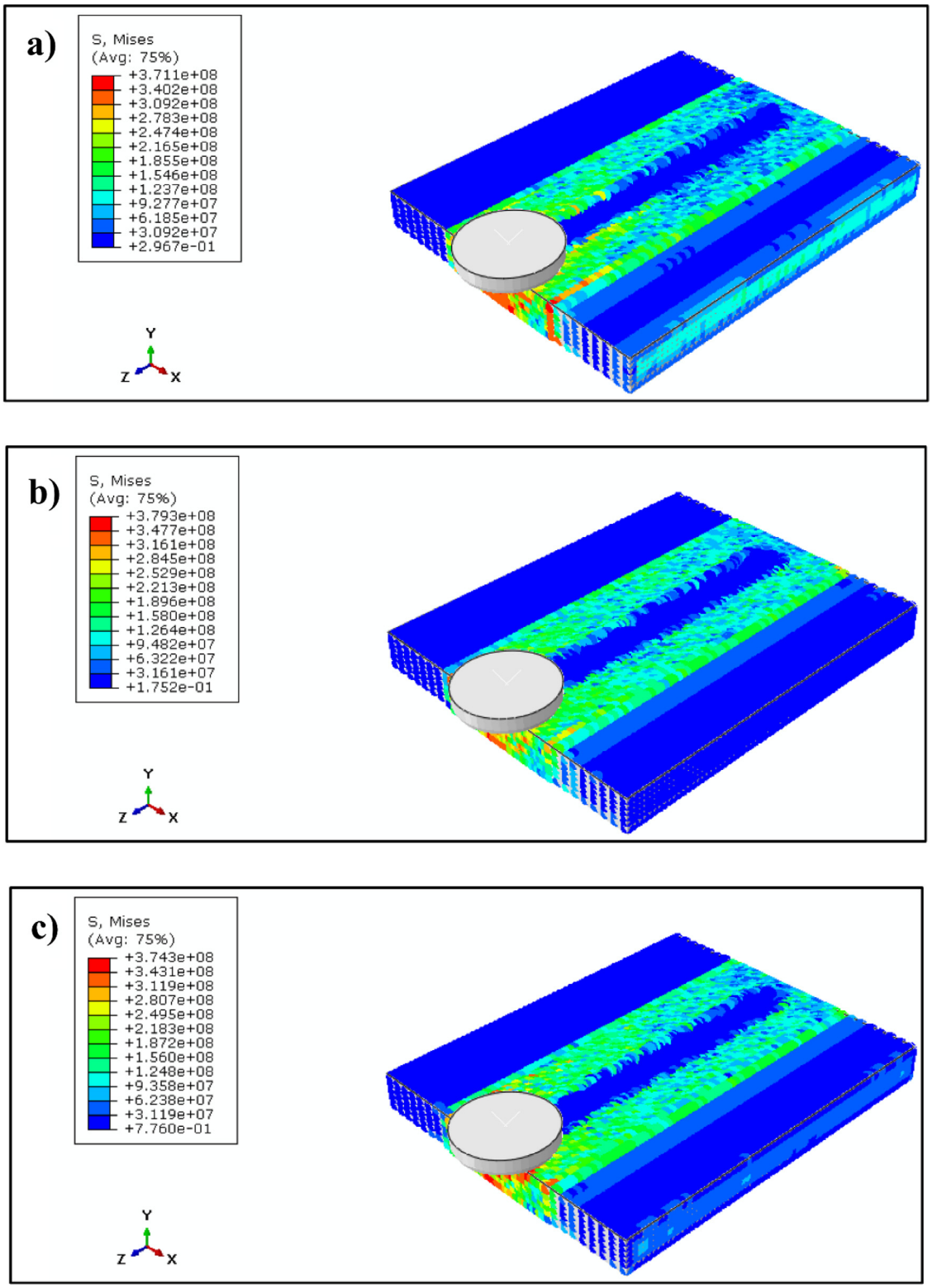

Fig. 10. Residual stress field (Pa) in the welded samples processed at constant moving speed of 150 mm/min and moving speeds of (a) 600 rpm, (b) 900 rpm and (c) 1200 rpm. (With preheat).

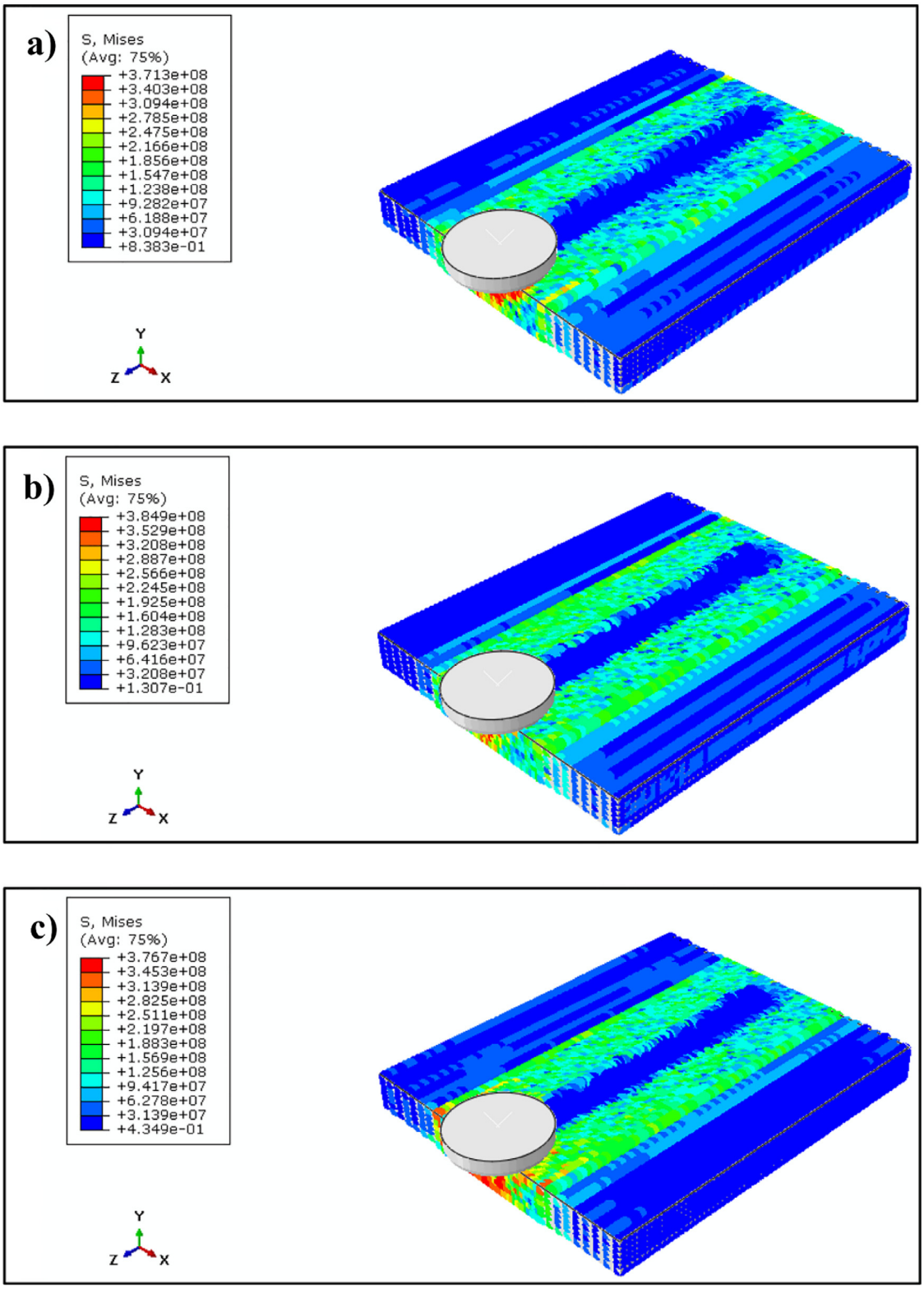

Fig. 11. Residual stress field (Pa) in the welded samples processed at constant moving speed of 150 mm/min and moving speeds of (a) 600 rpm, (b) 900 rpm and (c) 1200 rpm. (With preheat).

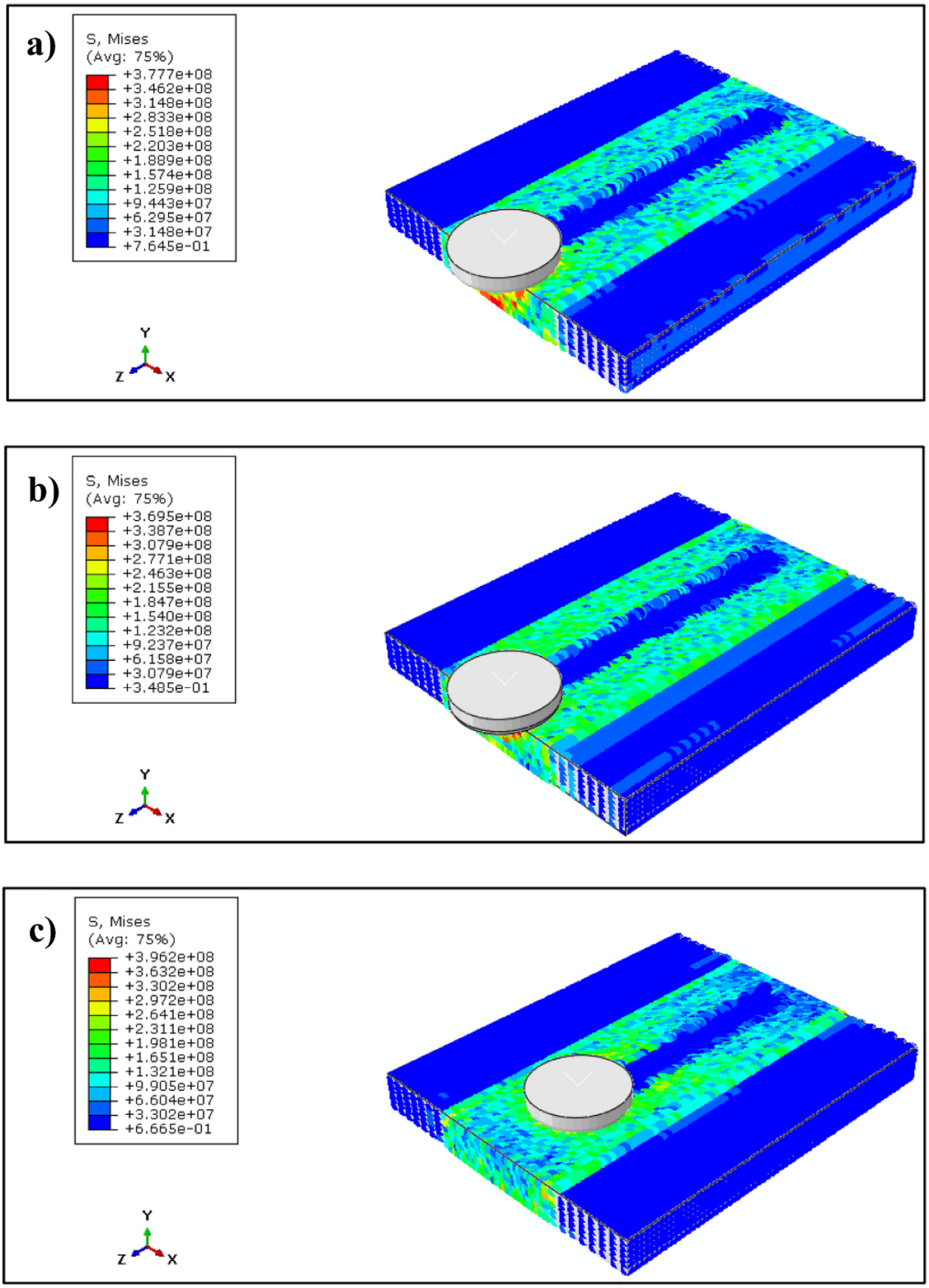

Fig. 12. Residual stress field (Pa) in the welded samples processed at constant moving speed of 150 mm/min and moving speeds of (a) 600 rpm, (b) 900 rpm and (c) 1200 rpm. (With preheat).

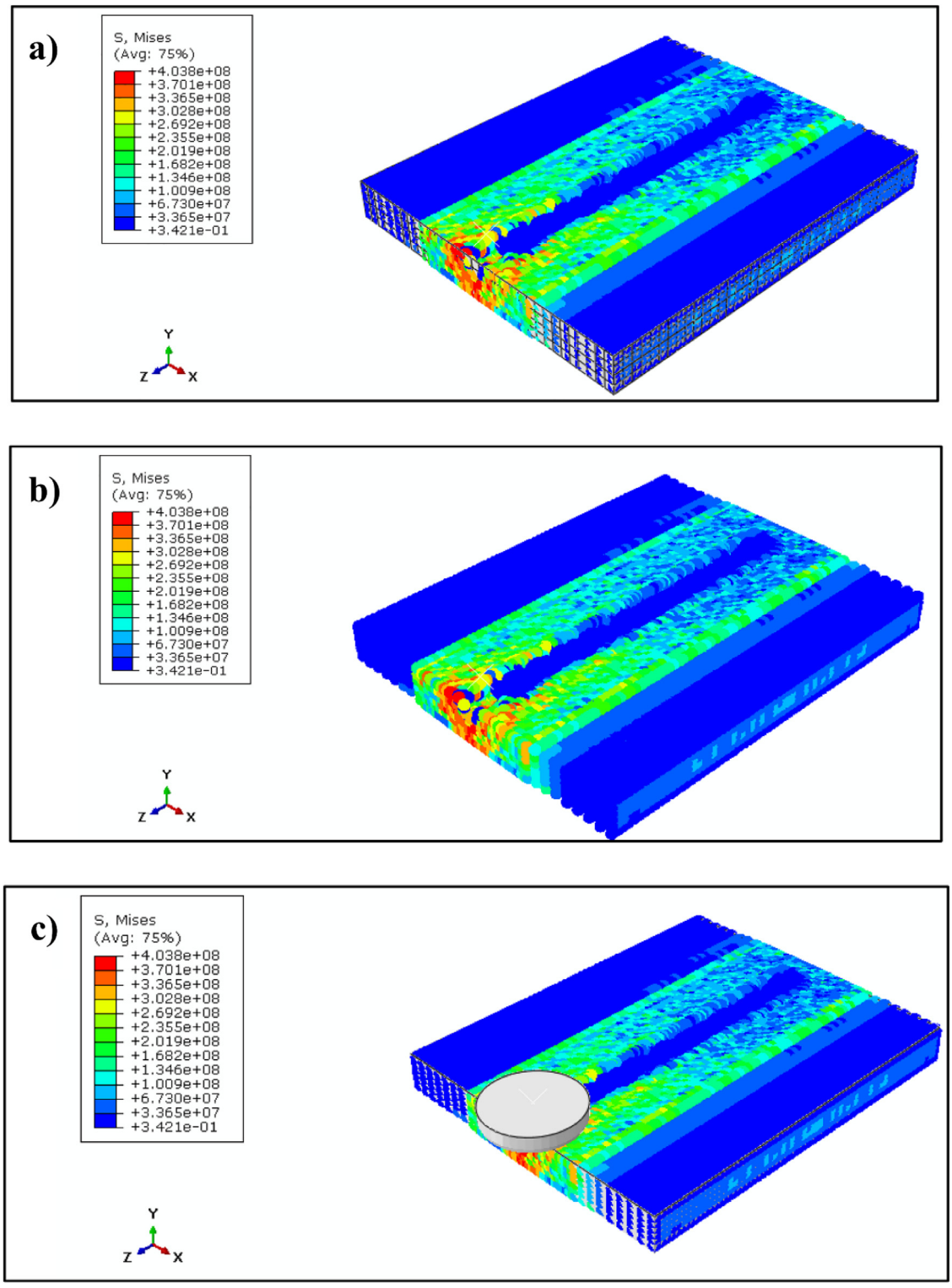

Fig. 13. Residual stress field (Pa) in the welded samples processed at constant rotational speed of 600 rpm and rotational speeds of (a) 50 mm/min, (b) 100 mm/min and (c) 150 mm/min. (No preheat).

in the distribution of residual stresses against the tool moving speed while the rotational speed is kept constant and without preheating. The corresponding stress for the same conditions with a 100 °C can be seen in Figs. 16–18. A decrease in longitudinal residual stresses can be distinguished with decrease in rotational speed, whereas not exactly the same trend was perceived in the case of transverse residual stresses with tool moving speed variation. A decreasing tool moving speed causes a higher amount of heat input in the material segment during FSW leading to a temperature rise in the as-welded

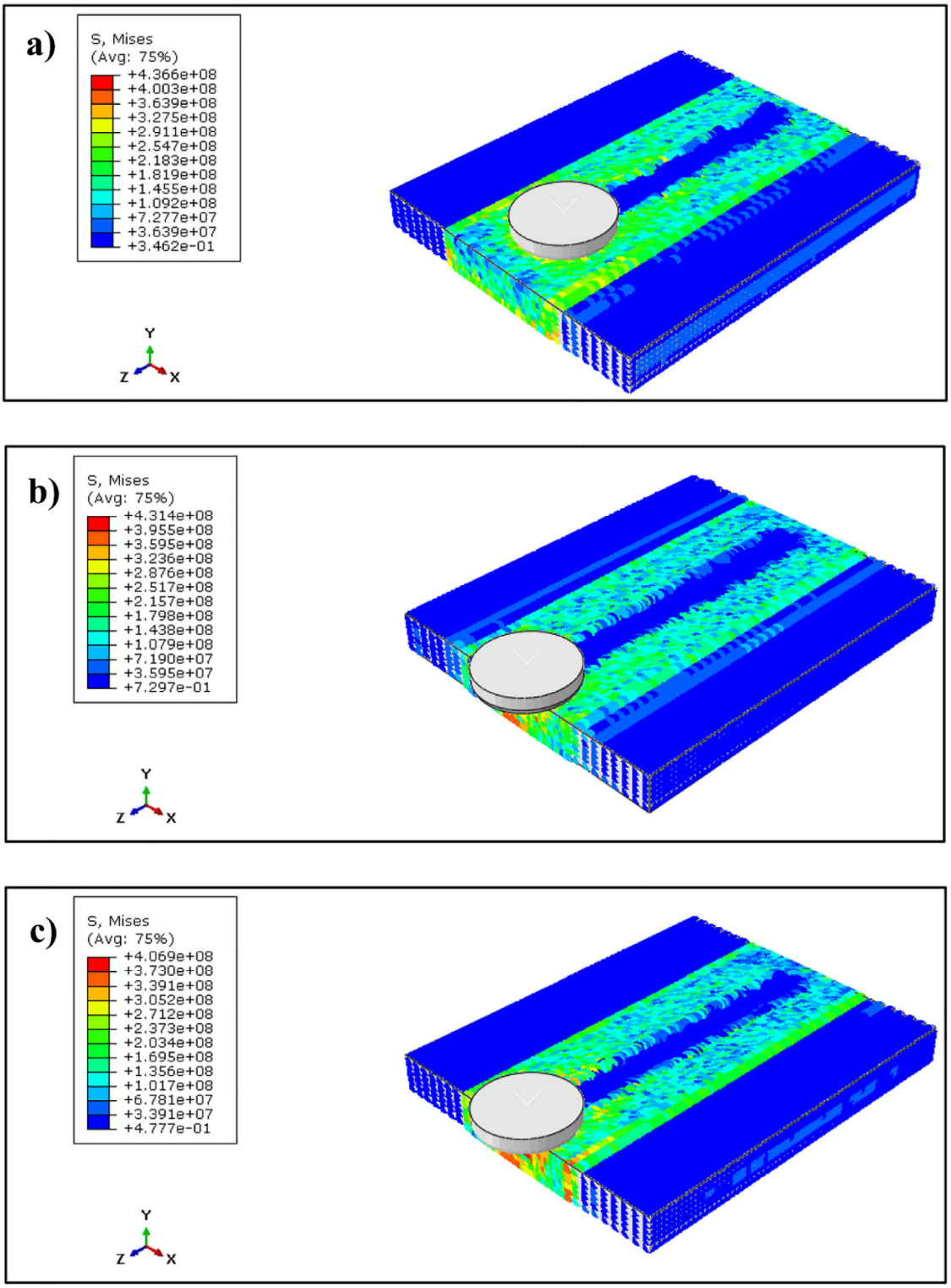

Fig. 14. Residual stress field (Pa) in the welded samples processed at constant rotational speed of 900 rpm and rotational speeds of (a) 50 mm/min, (b) 100 mm/min and (c) 150 mm/min. (No preheat).

sample. A higher peak temperature would result in a higher thermal stress relieving effect on the trailing crosswise of the rotating tool. As a result of the stress herelief reduced residual stresses are created at the lower tool rotation rate.

Fig. 19 illustrates the effect of preheating on residual stress in the samples with and without preheating before welding at a specific welding conditions, i.e. constant rotational and moving speeds. This figure can be considered as the representative for all other welding situations as the trend was the same comparing to other similar cases. In all the different combinations of the welding parameters, the magnitude of the residual stresses both in the longitudinal and transverse

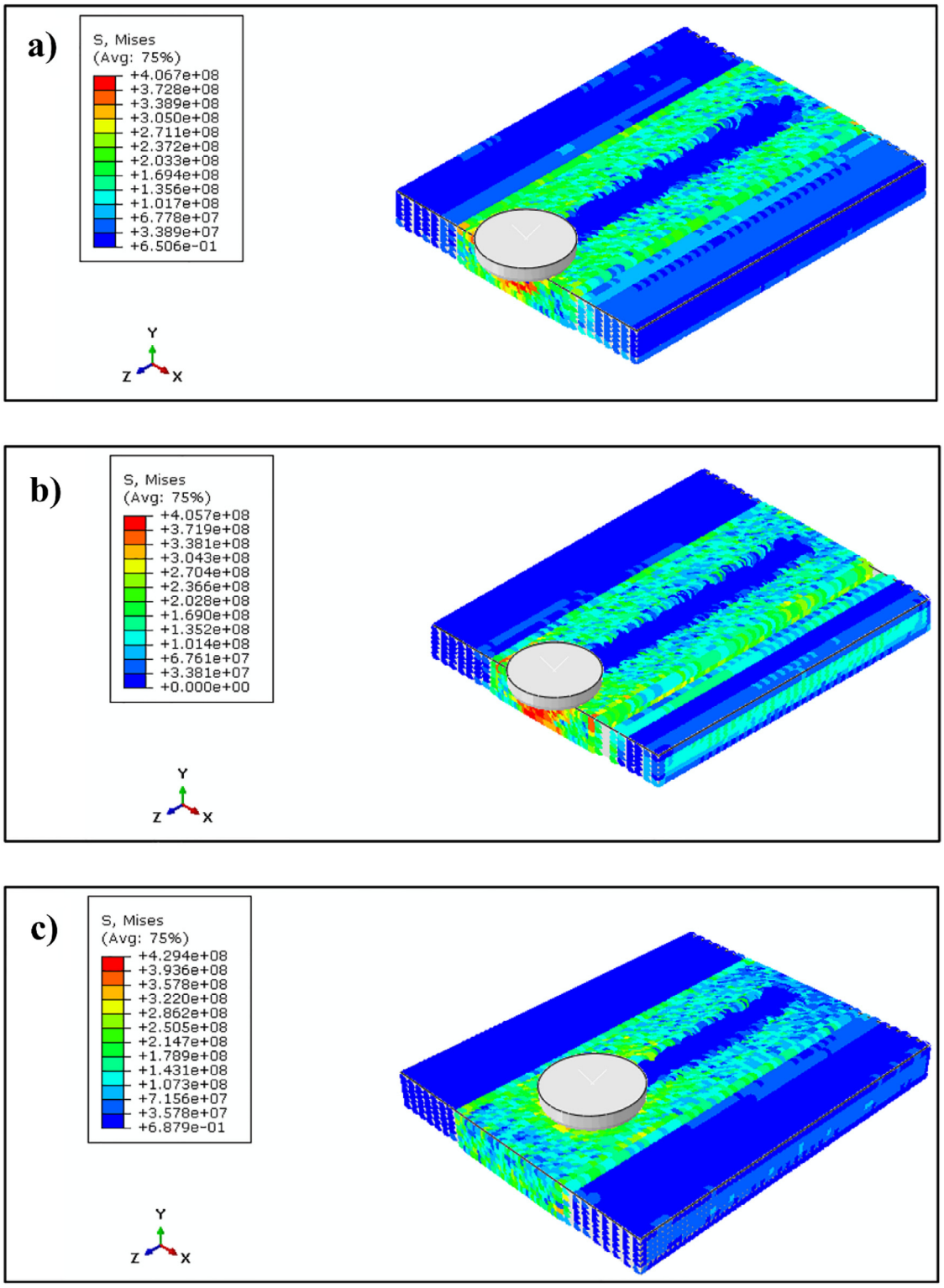

Fig. 15. Residual stress field (Pa) in the welded samples processed at constant rotational speed of 1200 rpm and rotational speeds of (a) 50 mm/min, (b) 100 mm/min and (c) 150 mm/min. (No preheat).

directions decreases with increasing of the preheating temperature. In the preheated samples, the heat generation stemmed of tool rotation form a less concentrated thermal ramp in the base metal and result in a more homogeneous material distortion. In the case, the stress in the zones around the tool is relatively lower than the material yield strength at a given temperature and it would be a weaker propensity for sample shrinkage as well. At the same conditions as with the case of no preheating, the adjacent material restrict the distortion recompense and therefore, residual tensile stresses are formed.

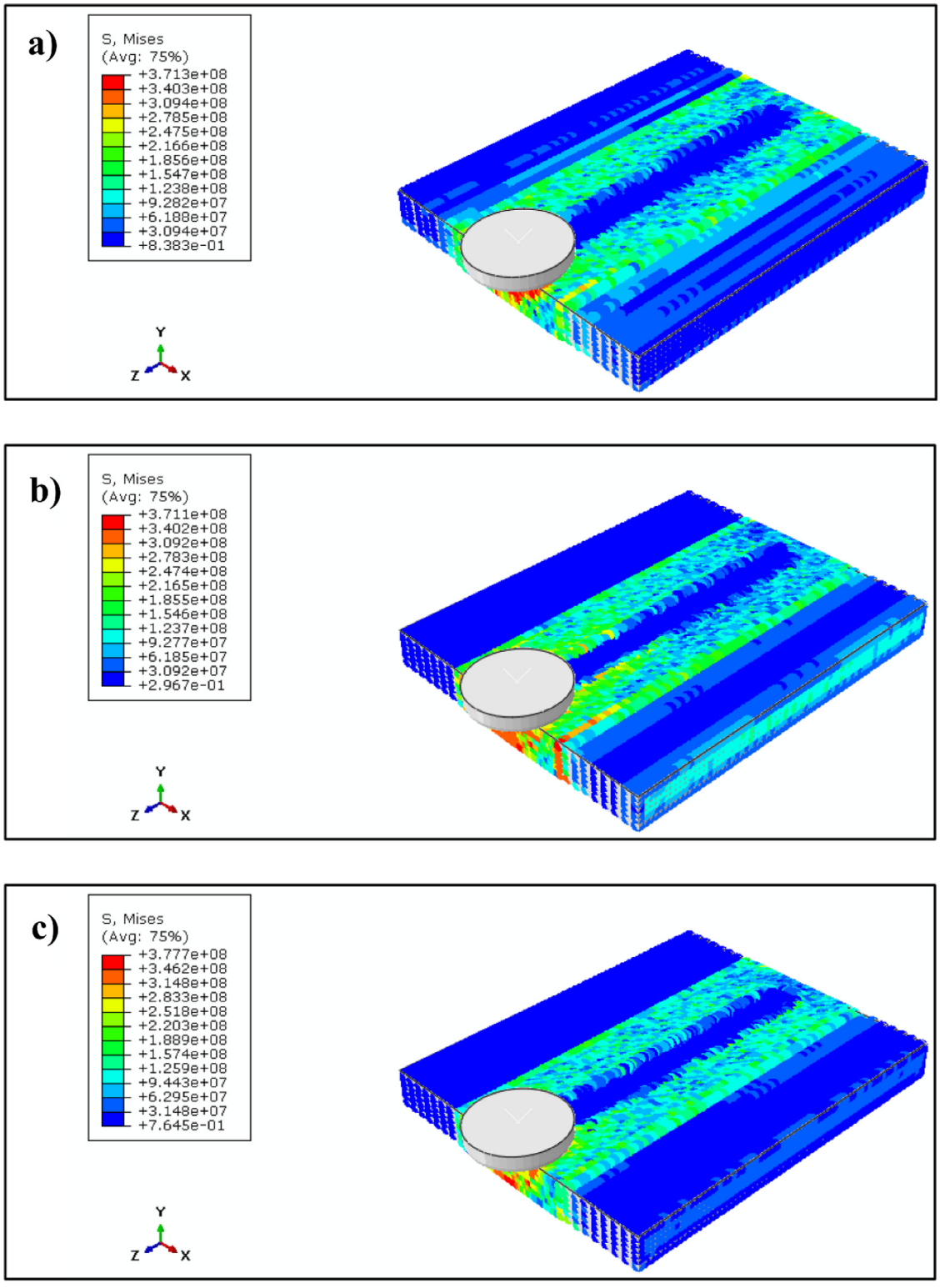

Fig. 16. Residual stress field (Pa) in the welded samples processed at constant rotational speed of 600 rpm and rotational speeds of (a) 50 mm/min, (b) 100 mm/min and (c) 150 mm/min. (With preheat).

Cooling rate is of contrariwise proportion with the preheating temperature which produces a ductile microstructure that increase resistance to weld cracking. Decrease in cooling rate, which yields ductile microstructure increase welded material resistance to cracking and also moderate shrinkage stress between the weld zone and base metal. Preventing chilling effect and ensuring about appropriate fusion, moisture elimination from the plat and enhanced tool lifetime can be other useful advantages of having the part preheated prior to FSW process.

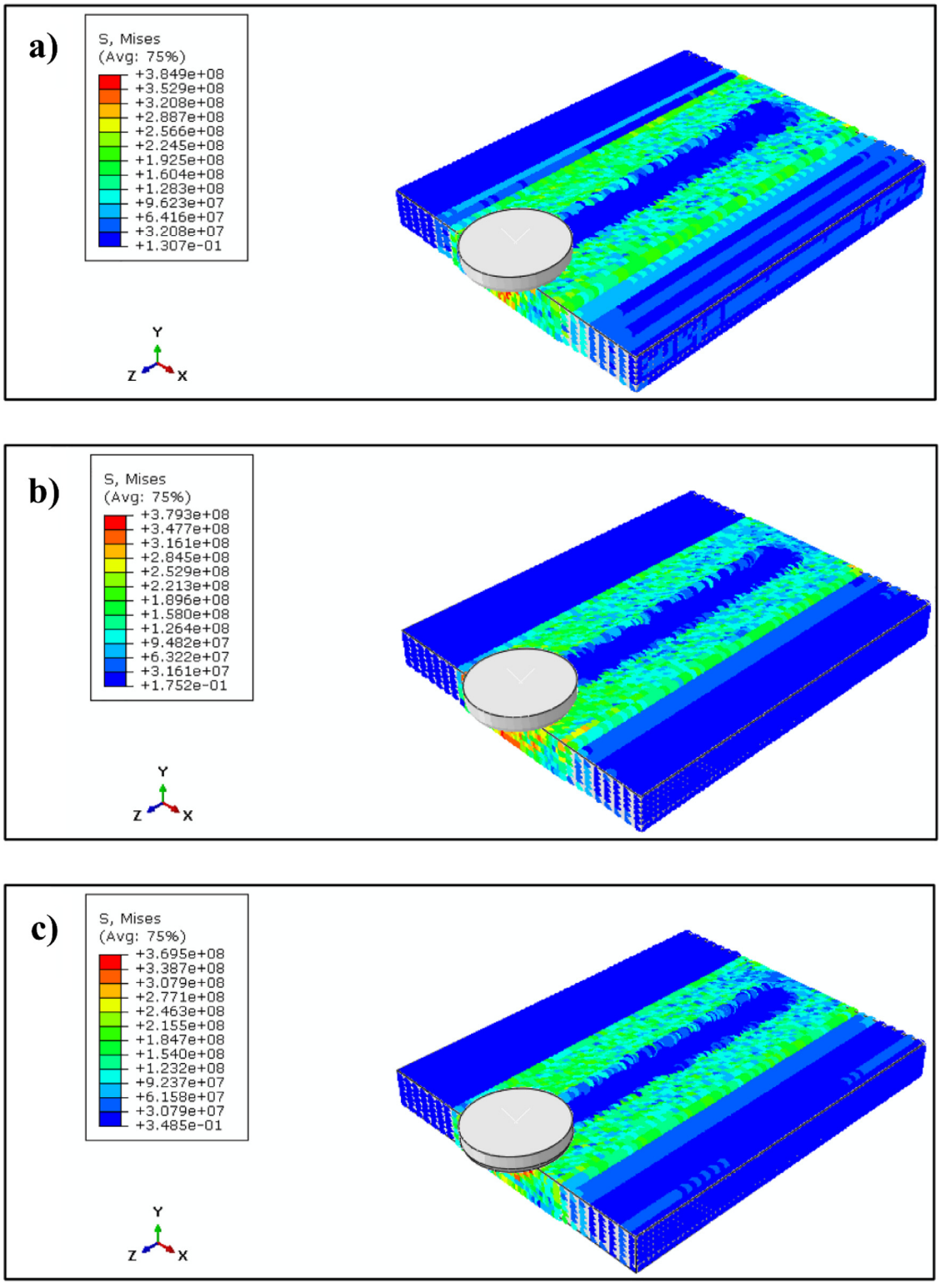

Fig. 17. Residual stress field (Pa) in the welded samples processed at constant rotational speed of 900 rpm and rotational speeds of (a) 50 mm/min, (b) 100 mm/min and (c) 150 mm/min. (With preheat).

4.3. FEM synchronization and quasi-static analysis

To preserve the accuracy in 3D FEM simulation of the FSW, considering the severe deformation using C3D8R elements, (eight nodes with three degrees of freedom in Cartesian space) element size should be selected. Although mesh is not the calculation unit in the SPH simulation, the number of nodes in the model and their concentration are controlled by

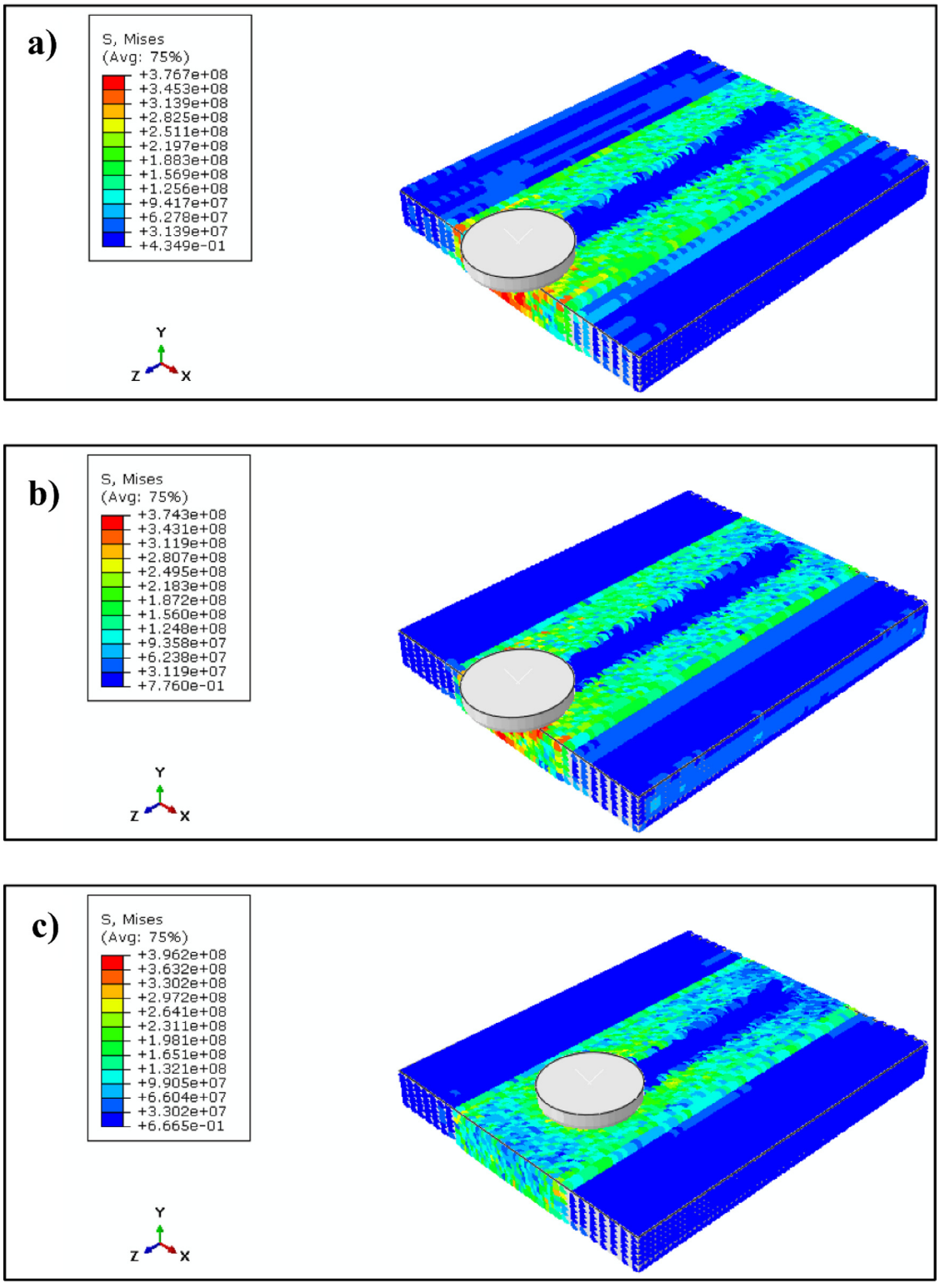

Fig. 18. Residual stress field (Pa) in the welded samples processed at constant rotational speed of 1200 rpm and rotational speeds of (a) 50 mm/min, (b) 100 mm/min and (c) 150 mm/min. (With preheat).

the mesh size. It is somehow guarantee the numerical solution convergence as well as independency of the results on the mesh arrangement. Accordingly, two welding conditions were selected to examine the element size dependency of simulation in which different mesh sizes were employed from fine to coarse. The selected models used as extreme cases are the ones with rotational speed of 1200, moving speed of 150 m/s, and with and without preheating. The size analysis ranged

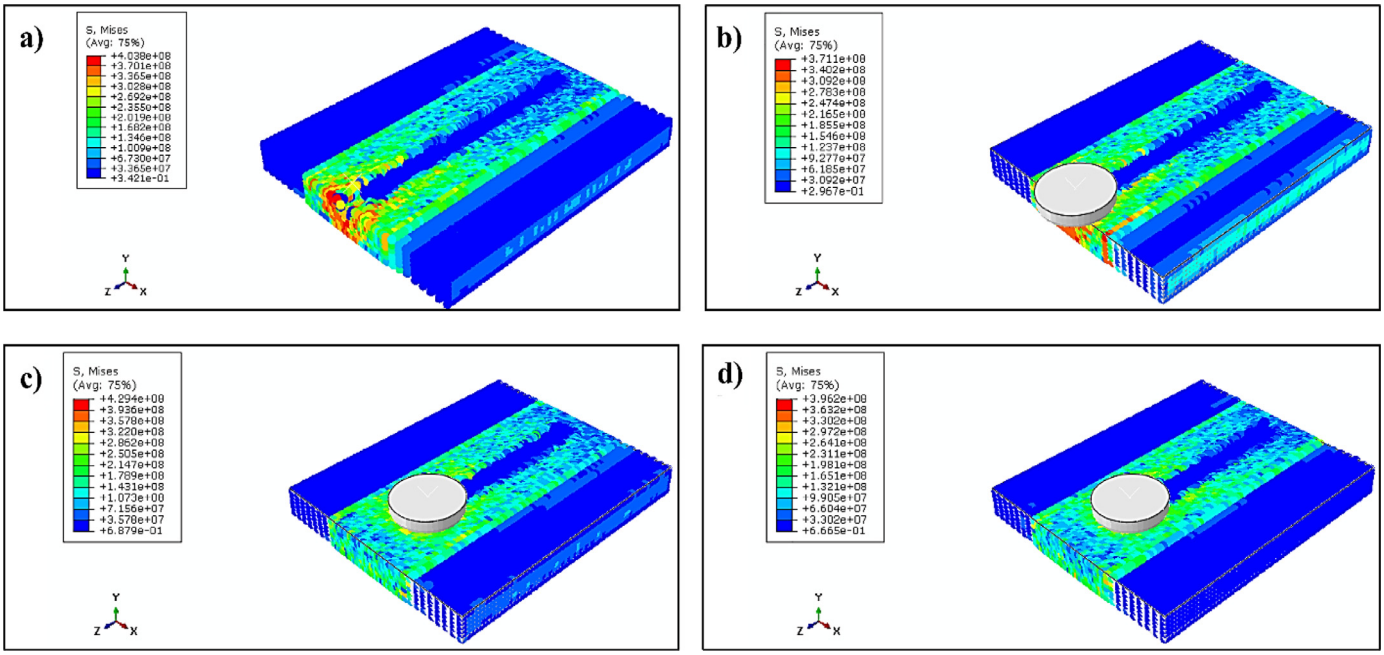

Fig. 19. Effect of preheating on residual stress field (Pa) in different welding conditions i.e. (a) rotational speed of 600 rpm - moving speed of 100 mm/min without preheat (b) rotational speed of 600 rpm - moving speed of 100 mm/min wit preheat (c) rotational speed of 1200 rpm - moving speed of 150 mm/min without preheat (d) rotational speed of 1200 rpm - moving speed of 150 mm/min wit preheat.

from 0.1 to 1 mm and evaluation of the size-dependency of maximum stress at the final stage of welding predicted that the mesh size of 0.4 could be used as the threshold for the mesh size independency and reliable stress analysis.

As the mass scaling utility was implemented to the model, a verification step is necessary to be performed to ensure preserving the accuracy while the computational cost of the simulation is reduced. The ratio of kinematic energy to overall internal energy for model was weighted against each other (Fig. 20). The satisfactory mass scaling factor for the analysis is achieved when the kinetic energy is less than ten percent of the total energy. As seen in Fig. 20, the ALLKE/ALLIE ratio for mass scaling of 1000 has an approximate maximum ratio of ten percent which means that the FSW can be determined as quasi-static case at the onset of the practice. It can be deduced that, using a value of 1000 for the mass scaling is not of significant influence on the accuracy of simulation result while CPU runtime become noticeably reduced.

4.4. ANFIS model for predicting residual stress of the friction stir welded AZ91 alloy

ANFIS is a high performance input-output mapping paradigm based on simultaneous adaptive learning ability of the nodes used in the ANN and logical rule-based inference patterns of the fuzzy logic. The schematic design of a typical ANFIS is presented in Fig. 21.

The details of the methodology for this adaptive system is defined throughout its five layer function activation as follows:

Layer 1 (Input layer): The membership functions (MF) of inputs that can get different shapes like triangle-shape,

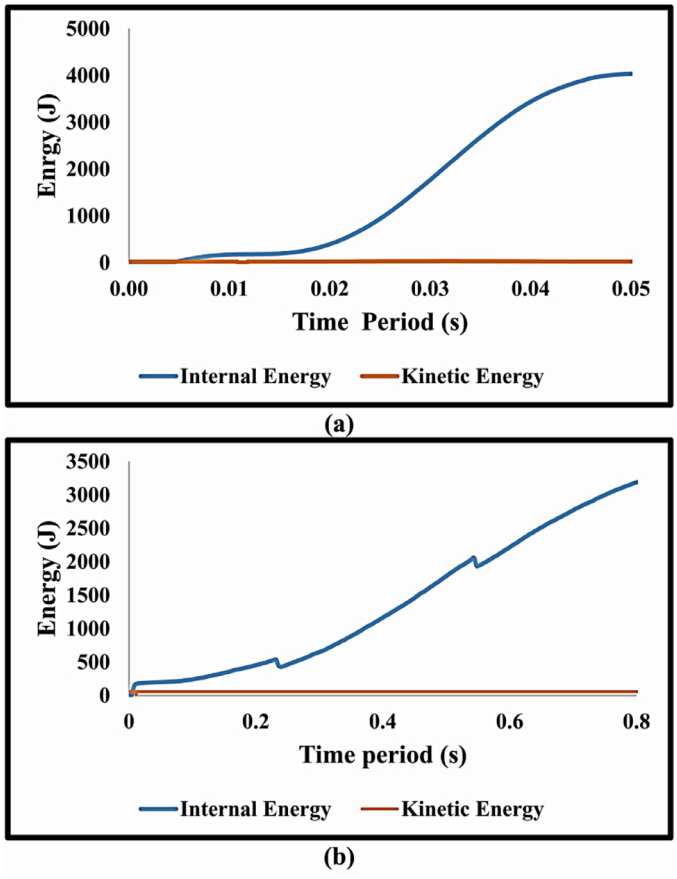

Fig. 20. Comparison of internal energy versus kinetic energy during the FSW at rotational speed of 1200 rpm and moving speed of 150 mm/s (a) without and (b) with preheating.

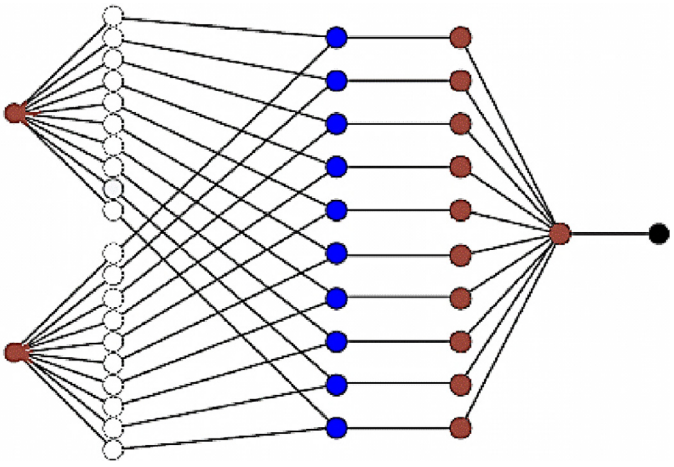

Fig. 21. Typical architecture of ANFIS model.

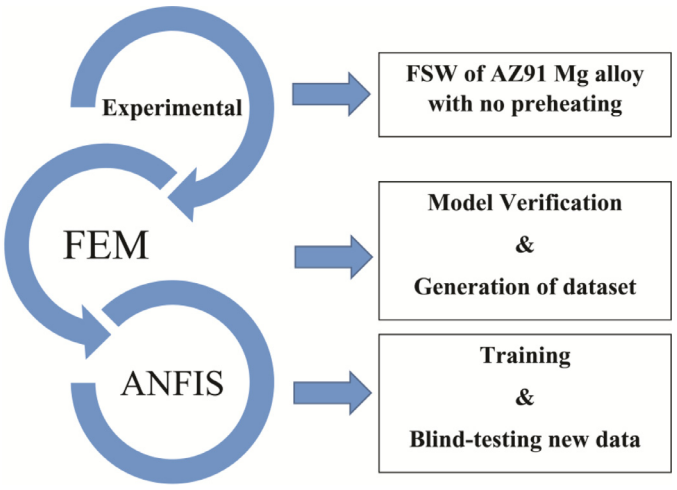

Fig. 23. The hybrid Experimental/ SPH/ ANFIS workflow for residual stress estimation.

bell-shape, trapezoid, or etc. The bell-shape MF was selected for the fuzzification of input and output data, according to Eq. (5):

$$F(x) = \frac{1}{1 + \frac{1}{\left[\left(\frac{x-a}{b}\right)^{c}\right]^{2}}} \tag{5}$$

Where a, b and c terms characterize the 'premise 'parameters of the defined function. Every MF transforms the crisp data to fuzzy ones by assigning membership degrees to every individual input.

Layer 2 (Product layer): In this layer, the incoming fuzzified signals are multiplied by each other and the outcome provides the attained terms as:

$$w_i = \mu_i(A) \times \mu_i(B) \tag{6}$$

where w_i represents the weight of the layer and μ_i terms are the MFs matching linguistic-based concept.

Layer 3 (Normalize layer): In the third layer, normalizing of the weight function happens by constructing $\bar{w}$ as the normalized weight value for n number of weights:

$$\bar{w} = \frac{w_i}{\sum_1^n w_i} \tag{7}$$

Layer 4 (Defuzzification layer): The defuzzification step takes place after summation of all involved weights are created:

$$O_i = \overline{w_i} f_i = \overline{w_i}\left(p_{x.}x + q_{y.}y + r_i\right) \tag{8}$$

in which, the three terms of p, q and r are known as the consequent parameters.

Layer 5 (Output layer): The total output is then calculated by taking a sum over all the incoming signals:

$$\bar{w} = \frac{w_i f}{\sum_1^n w_i f} \tag{9}$$

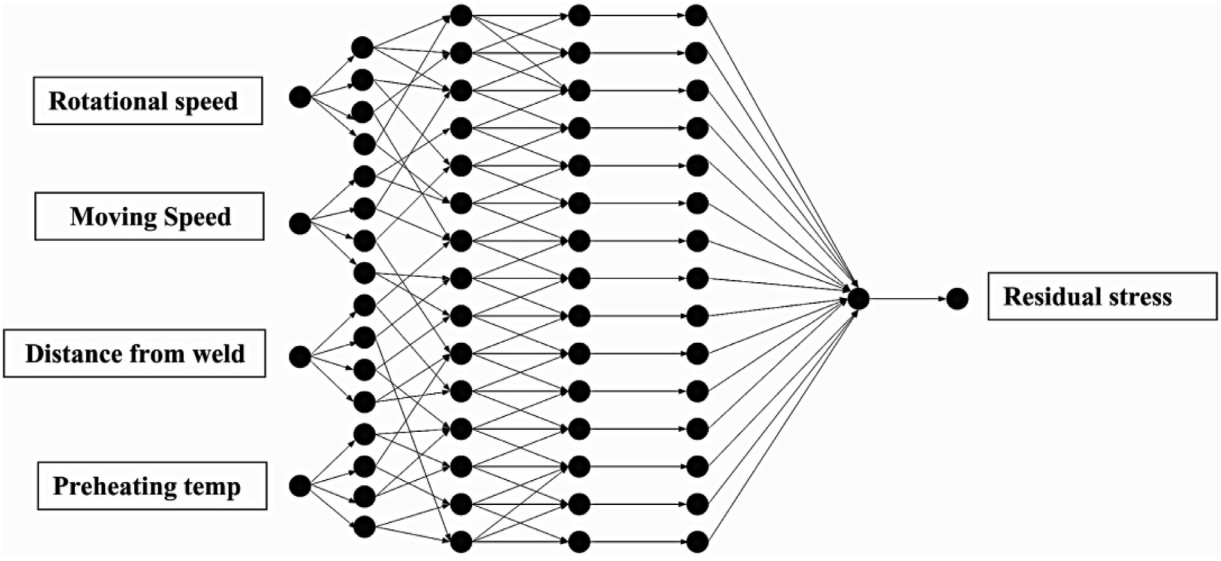

Fig. 22. The architecture of ANFIS for the prediction of residual stress during FSW of AZ91 alloy.

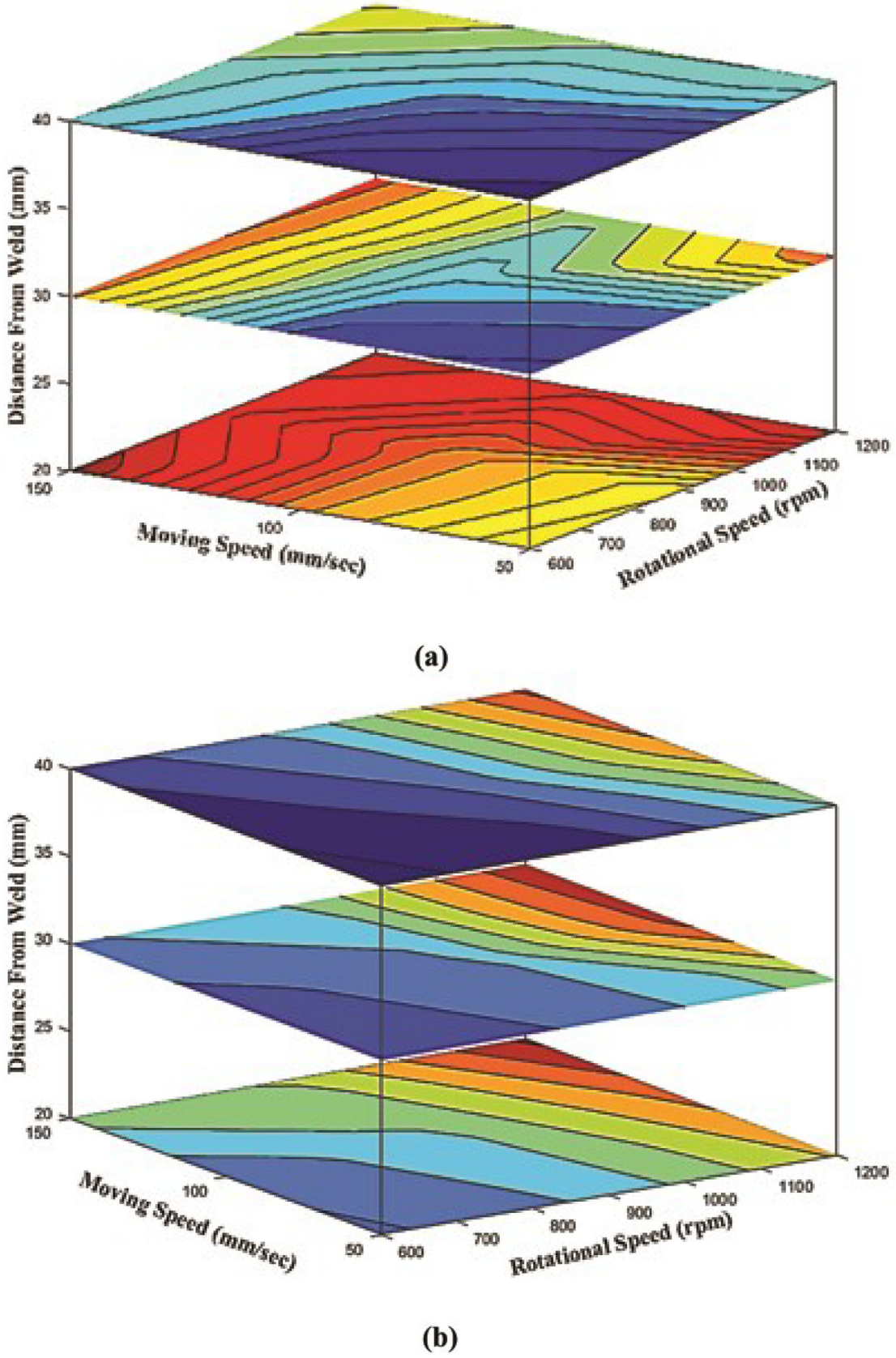

Fig. 24. Iso-stress contours for all possible welding assortments for those processed (a) with no preheating and (b) with a 100 °C preheating regime.

The ANFIS is mainly based on Takagi–Sugeno inference model and its training activity is performed by a set of hybrid learning regulations. The "premise" parameters are continuously restructured by back-propagation learning algorithm, and the "constant" parameters are recognized by the least mean squares approximation. The general output can be stated in terms of the combination of developed constant terms using Eq. (10):

$$f = \frac{w_1}{w_1 + w_2} f_1 + \frac{w_2}{w_1 + w_2} f_2 = \bar{w}_1 f_1 + \bar{w}_2 f_2 = \overline{w_1}(p_1.x + q_1 y + r_1) + \overline{w_2}(p_2.x + q_2 y + r_2) \quad (10)$$

which can be expressed in the matrix form of Eq. (11):

$$F = XW \quad (11)$$

In the training procedure, the premise factors of adaptive system are rationalized by the gradient descent method based on Eq. (12):

$$A_{mn}(n+1) - A_{mn}(n) = (L.R) \times \frac{\partial E}{\partial n} \quad (12)$$

$$E = \frac{(f_T - f)^2}{2} \quad (13)$$

where $(L.R)$ and E represent the learning rate and system energy, respectively and f_T and f (according to Eq. (10)) are targeted and predicted values. In order to establish the partial derivative of energy with respect to its dependent parameters, chain rule is applied to Eq. (7) in the form of Eq. (14):

$$\frac{dE}{da} = \left(\frac{\partial E}{\partial f}\right)\left(\frac{\partial f}{\partial w}\right)\left(\frac{\partial w}{\partial \mu}\right)\left(\frac{\partial \mu}{\partial a}\right) \quad (14)$$

By integrating and replacing Eq. (10) in Eq. (13), Eq. (14) can be restated in the form of Eq. (15):

$$\frac{dE}{da} = (f_T - f)\left(\frac{\partial (p_x.x + q_y.y + r_i)}{\partial w}\right)\left(\frac{\partial w}{\partial \mu}\right)\left(\frac{\partial \mu}{\partial a}\right) \quad (15)$$

The four inputs of ANFIS model for predicting residual stress are welding parameters i.e. rotational speed (n) and linear moving velocity (V)) together with distance form weld line center and preheating temperature. In the model, n gets the values of 600, 900 and 1200 rpm and V ranges from 50, 100 and 150 mm/min. The welding was performed in all the conditions with preheating temperature of 100 °C and without preheating and residual stress was measured at different distances of 40, 50, 60 and 70 mm from the weld center. The rotational speed, moving velocity, preheating temperature and distance from weld center are the ANFIS inputs and residual stress is the single output of the model. Based on the analysis described, the types of MF for all the four input variables are bell-shaped. The developed construction of ANFIS model to calculate the residual stress of the welded the AZ91 alloy is presented in Fig. 22.

To attain the experimental data required for validation of numerical simulation, two AZ91 Mg parts was welded by the FSW process at the same conditions implemented in one of the numerical simulations ($n = 900$ rpm - $V = 100$ mm/s – $T = 25$ °C) and the residual stresses were measured in the as-weld surface. The essential data for ANFIS learning are provided by a less overpriced technique like the numerical calculations. A numerical model of the FSW was established in the commercial finite element software, ABAQUS®, and results were compared with the experimental tests which were accomplished to authenticate the FEM model. A total 72 FEM run solutions were performed in order to acquire the required data for training and testing the ANFIS. The ANFIS is then developed in MATLAB® 2016 where it was trained by the data obtained from the finite element results of the residual stress. A well-trained ANFIS enabled to predict the previously seen data was blind-tested against new unseen data during the so-called testing phase. The hybrid methodology used in the present paper (Experimental, FEM and ANFIS) is schematically described in Fig. 23.

Fig. 24 shows the results of testing the integrated prediction outputs in all the possible combinations of training and testing data. 16 data were selected randomly in the range of the process input parameters to be used at the testing phase and the performance of model was evaluated by comparing

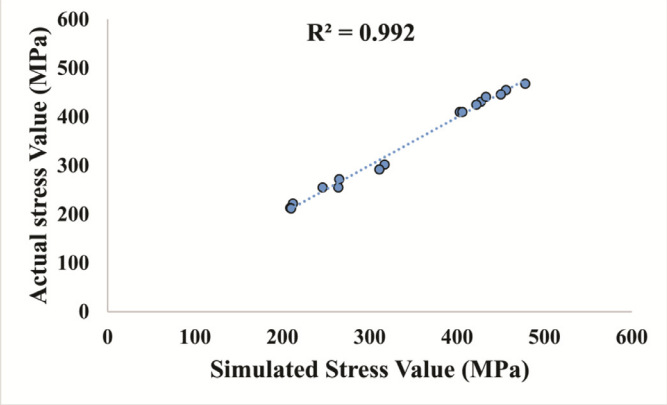

Fig. 25. Cross-validation of ANFIS results with experimental data.

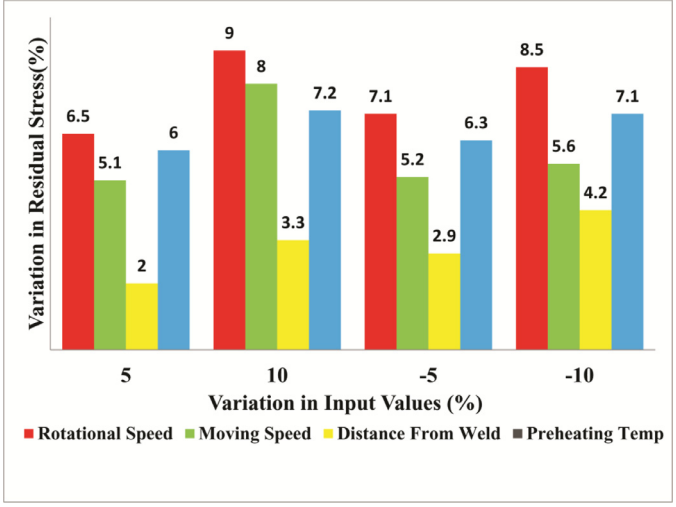

Fig. 26. Sensitivity analysis of residual stress to welding the parameters during FSW.

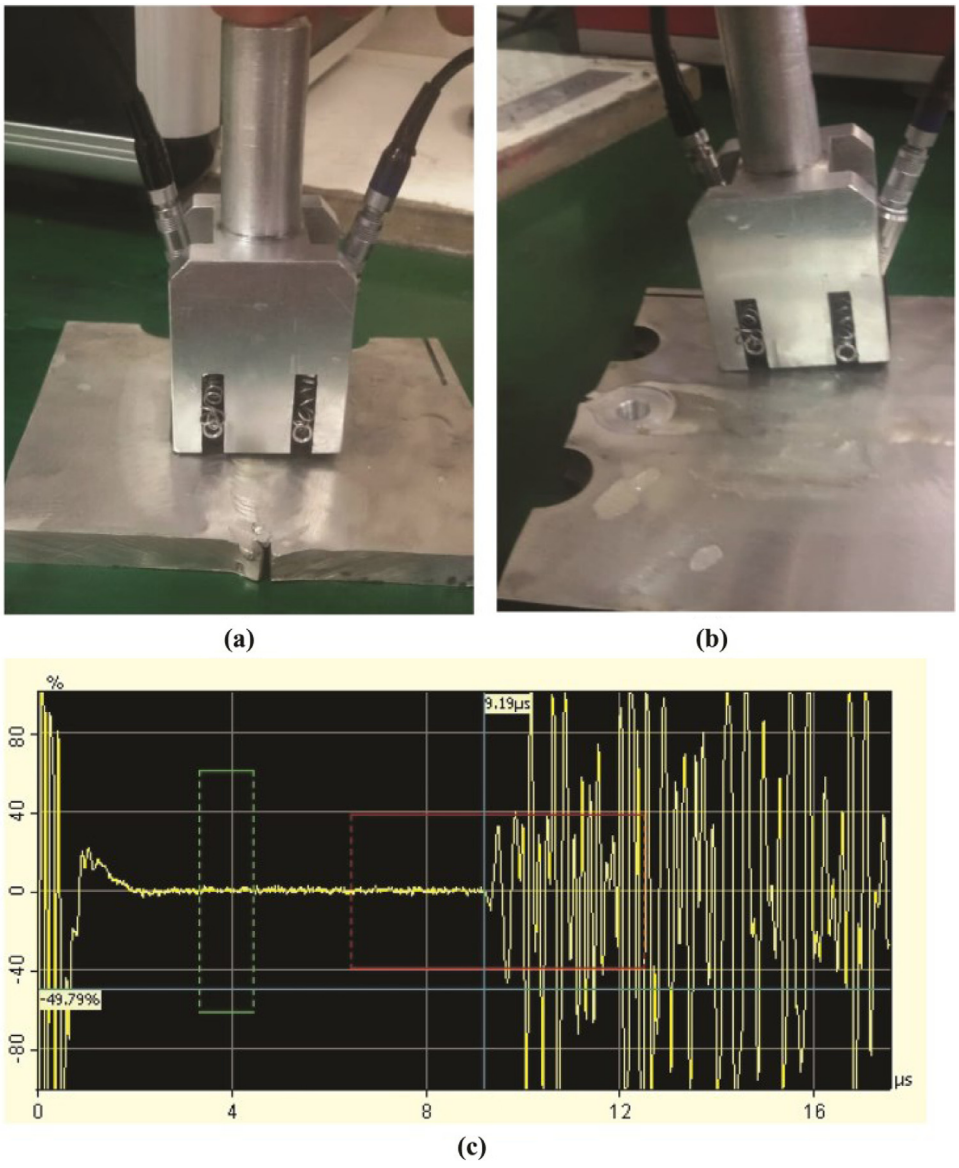

Fig. 27. Stress measurement at (a) weld line, (b) transverse direction and (c) reflected wave indications at 4 mm transverse distance from weld line.

ANFIS results with those obtained from validated SPH simulations (targets).

The regression line of the targets/outputs is shown in Fig. 25. As indicated, the assessed results are of an acceptable accuracy in the specified range, and finite element simulation.

4.5. Sensitivity analysis

Sensitivity analysis is typically carried out to study the sensitivity of the ANFIS model outputs to the inconsistency of input factors. In this research work, an attempt was made to regulate the influence and consequence of the FSW process parameter on residual stress of the welded samples. Keeping this in mind, the output variation were monitored as a function of incremental changing of the input parameter. The variation values of 5 and 10 were nominated for the model inputs and output was determined by the final well-trained ANFIS structure. The sensitivity of every individual input was then calculated by Eq. (16).

$$\text{Sensitivity level of } X_i(\%) = 1/N\sum_{j=1}^{N}\left(\frac{\%\text{Change in stress}}{\%\text{Change in welding parameter}}\right)_j \quad (16)$$

where N is the number of data-points.

Fig. 26 shows the results of the sensitivity analysis. Results show that the temperature has the greatest effect while strain rate and strain have comparatively less influence on high temperature mechanical properties of the samples.

4.6. Model verification: ultrasonic measurement of residual stress field

Based on the basic principles of acousto-elasticity, there exist a relation between the longitudinal wave velocity pro-

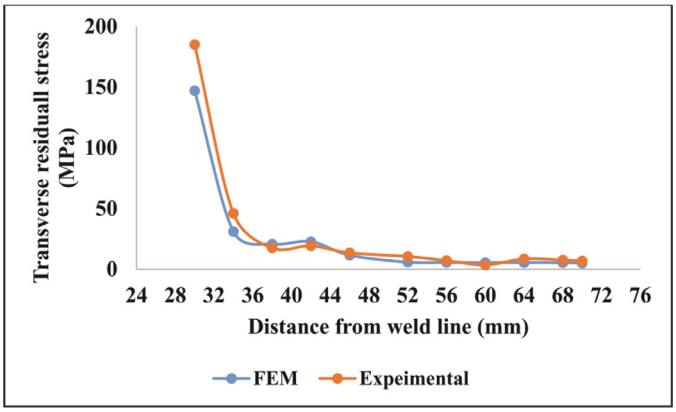

Fig. 28. Validation of the SPH model by using the ultrasonic wave measurement.

liferating alongside the stress track and the stress which is obtained. In the field test, the space between the sending and receiving transducer is constant and the sound velocity variation can be recognized by computing the adjustment of the sound time. As reported by [17], the correlation between the induced stress and the time change of sound transmission can be given by Eq. (17):

$$\frac{d\sigma}{dt} = -\frac{2}{K_\alpha t_0} \tag{17}$$

where K_α represents the stress coefficient and t_0 is the time required for the longitudinal wave to spread over a fixed distance with no transversally induced stress.

Once the longitudinal critical reflected wave is excited from a sending/receiving probe-pair at a certain depth of stable distance in component of finite thickness stress, the penetration depth of the wave is assumed to be a function of frequency (f). Javadi et al. [17] proposed that the detection depth (D) alters as the frequency of the excitation/receiving transducer fluctuates. The relationship between the depth and the frequency satisfies the following Eq. (18):

$$D = V \times f^{-0.96} \tag{18}$$

where D is the penetration depth of the wave, f is the sending/receiving transducer frequency and V is the velocity of the reflected wave in the sample. Taking the abovementioned relations and the distance between the two probes (L), the residual stress can be measured by ultrasonic testing. It should be noted that, some considerations such as surface roughness and geometry of component have to be considered and their effect have to be involved in the measurement. The probe installation and wave presentation in ultrasonic testing device can be seen in Fig. 27.

After calculation of appropriate setting and instrumental/calibration constant, the transmission and receiving period of the wave in the FSW samples, the resultant residual stress for each point of the weld zone can be calculated. The specimens are prepared by wire-cut electro-discharge machine to reduce the interference of unpredicted effects.

Fig. 28 shows that the distribution of longitudinal and transverse residual stress as compared to the simulated ones by the SPH approach. There is a good accordance between the simulated and experimentally measured residual stress in the directions of desire. This illustration verifies the accuracy and acceptable predictability of the SPH calculations in simulation of AZ91 FSW process. Some deviations, however, are observed in the results that can be attributed to both the round-up task of FEM solver and the ultrasonic pulses resolution that cannot preserve the accuracy in measuring the microscale stresses caused by heterogeneity of the microstructure or grain misorientation.

5. Conclusions

A combined approach of experimental, smoothed particle hydrodynamic and neuro-fuzzy inference system were utilized to predict the residual stress of friction stir welded AZ91 part by varying its welding/preheating parameters. A number of conclusions can be drawn from the analysis and discussions:

- Unlike the conventional element-based methods, SPH as a Lagrangian particle technique can simulate the welding dynamics, severe plastic deformation, and the induced stress history without any need for the intricate tracking patterns.
- With the data obtained from the ultrasonic testing, a very good agreement was found between results of the SPH simulation for residual stress proving the potential of the proposed model.
- The effect of all the involved welding parameters and the preheating temperature on the residual stress and their sensitivity was investigated using results of the numerical SPH simulation and neuro-fuzzy system.
- The Johnson–Cook constant parameters for AZ91 Mg alloy was determined by using non-linear least square fitting method to be implemented in the SPH framework as the material model.
- The ANFIS has been trained by a virtual testing campaign accomplished by the SPH model. It provides acceptable errors both in the learning and the testing validation cases. The optimum results have been obtained with Gaussian membership functions for all the inputs.
- The proposed combined methodology allows developing an ANFIS that efficaciously predict residual stress of welded AZ91 with different FSW parameters. This hybrid numerical-soft computational model, authenticated by ultrasonic tests, is capable to mimic the effect of the operational/temperature factors on the residual stress distribution.

Conflict of Interest statement

The authors declare that they have no conflict of interest.

Supplementary material

Supplementary material associated with this article can be found, in the online version, at doi:10.1016/j.jma.2020.11.018.

References

[1] S. Mironov, Y.S. Sato, H. Kokawa, Metall. Mater. Trans. A 50 (6) (2019) 2798–2806, doi:10.1007/s11661-019-05194-0.
[2] A. Kouadri-Henni, L. Barrallier, Metall. Mater. Trans. A 45 (11) (2014) 4983–4996, doi:10.1007/s11661-014-2381-3.
[3] E. Cerri, P. Leo, P. De Marco, J. Mater. Process. Technol. 189 (1–3) (2007) 97–106.
[4] R.S. Mishra, Z. Ma, Mater. Sci. Eng.: R: Rep. 50 (1–2) (2005) 1–78.
[5] R. Nandan, T. DebRoy, H. Bhadeshia, Prog. Mater. Sci. 53 (6) (2008) 980–1023.
[6] Z.Y. Ma, Metall. Mater. Trans. A 39 (3) (2008) 642–658, doi:10.1007/s11661-007-9459-0.
[7] P. Threadgill, A. Leonard, H. Shercliff, P. Withers, Int. Mater. Rev. 54 (2) (2009) 49–93.
[8] G. Bhargava, W. Yuan, S. Webb, R.S. Mishra, Metall. Mater. Trans. A 41 (1) (2010) 13.
[9] N. Balasubramanian, R. Mishra, K. Krishnamurthy, J. Mater. Process. Technol. 209 (8) (2009) 3696–3704.
[10] G. Buffa, L. Fratini, S. Pasta, R. Shivpuri, CIRP Ann. 57 (1) (2008) 287–290.
[11] G. Bussu, P. Irving, Int. J. Fatigue 25 (1) (2003) 77–88.
[12] A. Steuwer, S.J. Barnes, J. Altenkirch, R. Johnson, P.J. Withers, Metall. Mater. Trans. A 43 (7) (2012) 2356–2365, doi:10.1007/s11661-011-0643-x.
[13] M.E. Kartal, F.P. Dunne, A.J. Wilkinson, Acta Mater. 60 (13–14) (2012) 5300–5310.
[14] H. Coules, D. Smith, K.A. Venkata, C. Truman, Int. J. Solids Struct. 51 (10) (2014) 1980–1990.
[15] W. Xu, J. Liu, H. Zhu, Mater. Des. 32 (4) (2011) 2000–2005.
[16] O. Hatamleh, I.V. Rivero, A. Maredia, Metall. Mater. Trans. A 39 (12) (2008) 2867–2874.
[17] Y. Javadi, M. Akhlaghi, M.A. Najafabadi, Mater. Des. 45 (2013) 628–642.
[18] H. Lu, X. Liu, J. Yang, S. Zhang, H. Fang, Sci. Technol. Weld. Join. 13 (1) (2008) 70–74.
[19] S. Gachi, F. Belahcene, F. Boubenider, Nondestr. Test. Eval. 24 (3) (2009) 301–309.
[20] M. Cervera, M. Chiumenti, Q. Valverde, C.A. de Saracibar, Comput. Methods Appl. Mech. Eng. 192 (49–50) (2003) 5249–5263.
[21] F. Al-Badour, N. Merah, A. Shuaib, A. Bazoune, J. Mater. Process. Technol. 213 (8) (2013) 1433–1439.
[22] M. Liu, G. Liu, Arch. Comput. Methods Eng. 17 (1) (2010) 25–76.
[23] J.J. Monaghan, J. Comput. Phys. 110 (2) (1994) 399–406.
[24] P. Cleary, J. Ha, M. Prakash, T. Nguyen, Appl. Math. Model. 30 (11) (2006) 1406–1427.
[25] P.W. Cleary, R. Das, in: Proceedings of IUTAM Symposium on Theoretical, Computational and Modelling Aspects of Inelastic Media, Springer, 2008, pp. 287–296.
[26] P. Cleary, M. Prakash, J. Ha, J. Mater. Process. Technol. 177 (1–3) (2006) 41–48.
[27] F. Jiang, M.S. Oliveira, A.C. Sousa, Comput. Phys. Commun. 176 (7) (2007) 471–480.
[28] S. Li, W.K. Liu, Appl. Mech. Rev. 55 (1) (2002) 1–34.
[29] P. Randles, L.D. Libersky, Comput. Methods Appl. Mech. Eng. 139 (1–4) (1996) 375–408.
[30] J.J. Monaghan, Annu. Rev. Astron. Astrophys. 30 (1) (1992) 543–574.